ABSTRACT

PRODUCTION OF NANOCRYSTALLINE NITRAMINE ENERGETIC MATERIALS BY RAPID EXPANSION OF SUPERCRITICAL SOLUTIONS

by
Victor Stepanov

Nanotechnology is a rapidly evolving field and has been characterized as "the next industrial revolution". Nanostructured materials are receiving increasing amount of attention in fields ranging from electronics to metallurgy due to their novel and unique properties. This work was focused on exploring the benefits of nanofabrication of high density energetic materials. The work primarily focused on the feasibility and viability of recrystallization of nitramine explosives down to the nanometer crystal size (<100 nm). It is anticipated that properties of the high density energetic materials such as sensitivity, packing density, crystal quality, energetic performance will be benefited.

Rapid Expansion of Supercritical Solutions was chosen as the process most appropriate to realize the objective. Solubility of CL-20 in supercritical solutions was studied. Nitramine crystals with sizes ranging from 100 to 3000 nm were produced having narrow size distribution. Effects of process conditions crystal size and shape were investigated. A continuous process was developed. Sum-gram quantities of nano-scale powders were produced.

PRODUCTION OF NANOCRYSTALLINE NITRAMINE ENERGETIC MATERIALS BY RAPID EXPANSION OF SUPERCRITICAL SOLUTIONS

by
Victor Stepanov

A Thesis
Submitted to the Faculty of
New Jersey Institute of Technology
in Partial Fulfillment of the Requirements for the Degree of
Master of Science in Chemical Engineering

Department of Chemical Engineering

August 2003

APPROVAL PAGE

PRODUCTION OF NANOCRYSTALLINE NITRAMINE ENERGETIC MATERIALS BY RAPID EXPANSION OF SUPERCRITICAL SOLUTIONS

Victor Stepanov

Dr. Lev N. Krasnoperov, Thesis Advisor — Date
Professor of Chemistry, NJIT

Dr. Dana E. Knox, Committee Member — Date
Associate Professor of Chemical Engineering and Environmental Science, NJIT

Dr. Robert Pfeffer, Committee Member — Date
Distinguished Professor of Chemical Engineering, NJIT

BIOGRAPHICAL SKETCH

Author: Victor Stepanov

Degree: Master of Science

Date: August 2003

Undergraduate and Graduate Education:

- Master of Science in Chemical Engineering
  New Jersey Institute of Technology, Newark, NJ, 2003

- Bachelor of Science in Chemical Engineering
  New Jersey Institute of Technology, Newark, NJ, 2000

Major: Chemical Engineering

Publications:

V. Stepanov, R. Damavarapu, and L. N. Krasnoperov, "A Novel Approach to Crystallization of Nano-scale Particles of High Density Energetic Materials," in *Proceedings of the 8th Meeting on Supercritical Fluids*, Bordeaux, France, pp. 451, April 2002.

E. M. Glebov, L. G. Krishtopa, V. Stepanov, and L. N. Krasnoperov, "Kinetics of a Diels-Alder Reaction of Maleic Anhydride and Isoprene in Supercritical CO_2," *J. Phys. Chem. A*, vol. 105, pp. 9427-9435, 2001.

L. N. Krasnoperov, and V. Stepanov, "Introduction of Laser Photolysis-Transient Spectroscopy in an Undergraduate Physical Chemistry Laboratory: Kinetics of Ozone Formation," *J. Chem. Ed.* vol. 76, pp. 1182-1183, Sept. 1999.

To my beloved family

ACKNOWLEDGEMENT

I wish to express my gratitude to Dr. Lev Krasnoperov for his support as the thesis advisor. His knowledge and insight helped guide this effort and taught me countless valuable lessons. Also, I would like to thank Dr. Dana Knox and Dr. Robert Pfeffer for their support and participation as the members of the thesis committee.

This work was sponsored by the US Army.

TABLE OF CONTENTS

TABLE OF CONTENTS
(Continued)

LIST OF TABLES

LIST OF FIGURES

LIST OF FIGURES
(Continued)

Figure **Page**

CHAPTER 1

INTRODUCTION

Novel high energy density materials such as octahydro-1,3,5,7-tetranitro-1,3,5,7-tetrazocine (HMX), hexahydro-1,3,5-trinitro-1,3,5-triazine (RDX), and 2,4,6,8,10,12-hexanitrohexaazaisowurtzitane (CL-20) show superior energetic performance with respect to their predecessor trinitrotoluene (TNT). However, their utilization is greatly limited due to the high sensitivity of these materials to external stimuli such as impact. High sensitivity renders these materials dangerous in many potentially useful military applications. The desired next generation energetic compounds would possess the energy density of CL-20 while having low sensitivity, comparable to that of TNT.

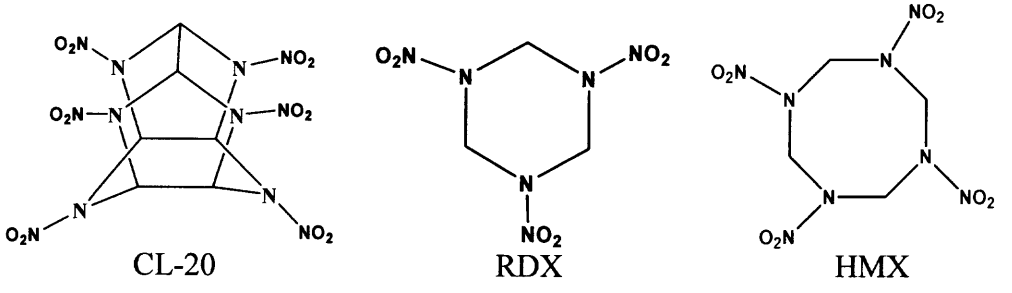

Figure 1.1 Chemical structures of CL-20, RDX, and HMX.

Numerous efforts are under way to synthesize new energetic compounds that would meet the energy and sensitivity requirements, but actual discoveries of useful materials are rare. Only a handful of materials that have the potential to replace TNT have been synthesized. Majority of these materials are of limited use due to their high sensitivity.

Alternatively, efforts are also being devoted to the improvement of the characteristics of existing materials. One of such methods is the introduction of various

coatings on the surfaces of the energetic crystals. Coatings have a very positive effect on sensitivity, however, they come at a price of reduced energy density, altered performance during detonation or deflagration, and increased production costs. Another approach which has received much attention is focused on the improvements in the crystal morphology (quality, size, etc). Such approach is the focus of the work presented in this thesis.

A number of standard tests are used in the explosives community to gauge the sensitivity of the energetic material. These tests measure the response of the energetic materials to external stimuli such as friction, static discharge, impact, short and long duration shock wave and more. These tests are used to characterize new materials and determine their applicability.

The effects of crystal characteristics on the sensitivity are profound and have been widely examined. Certain crystal characteristics such as the crystal shape, morphology, size, size distribution, internal inclusions and cavities, internal defects, and external defects are suspected of influencing the sensitivity and performance of energetic materials. Internal inclusions or cavities are very common in crystals formed using conventional organic processing techniques. Cavity sizes are typically on the order of 1 to 10 microns. Adiabatic compression of cavities during a shock wave propagation results in hot spot generation. Consequently, the hot spots lead to the initiation of the explosive material and detonation. Thus a key task in reducing the sensitivity is elimination of any intracrystalline inclusion.

Traditionally inclusions are eliminated from energetic materials by wet or dry milling techniques. This involves the physical grinding of the crystals into smaller (<10

μm) crystals with little or no residual inclusions. Such processing often results in a material of reduced sensitivity. However, certain materials, i.e. CL-20, are further sensitized by the milling process. This increase in sensitivity is believed to result from the sensitizing of the crystal surfaces due to the formation of imperfections on the crystal surface. Highly strained surface edges are formed by grinding and are more susceptible to breakage and initiation. A process is thus required which not only eliminates intracrystalline cavities but which also produces a stable crystal surface.

Most of the trends in crystal sensitivity with respect to size show the reduction of sensitivity with the reduction in crystal size. However, it is unknown whether this desensitization is strictly a result of size reduction. The changes in the crystal internal and external structure due to processing which results in smaller crystals may also have significant effects on the powder sensitivity. Sole size effects are not clear at the micron level, however, it is postulated that the interaction of the shock wave with the crystal may be dramatically altered when the crystal size becomes smaller than the width of shock wave. Thus, a critical crystal size can be anticipated below which sensitivity may take a dramatic decline.

Crystal size may also affect the morphology of the intercrystalline microstructure of the energetic material. Crystal packing arrangements and the size of intercrystalline voids may all be significant in shock wave / powder interaction dynamics.

In a recent effort it was shown that submicron crystals of RDX and HMX are significantly less sensitive than the larger crystals. Impact sensitivity was measured for the standard and recrystallized submicron HMX and RDX. A standard Army ERL impact test was used. In this test a 2.5 kg weight is dropped on a small sample of the explosive

powder. The test is repeated numerous times, each time adjusting the drop height. The test is aimed at finding the drop height where the explosive material undergoes initiation 50 % of the time. The results are illustrated in Figure 1.2.

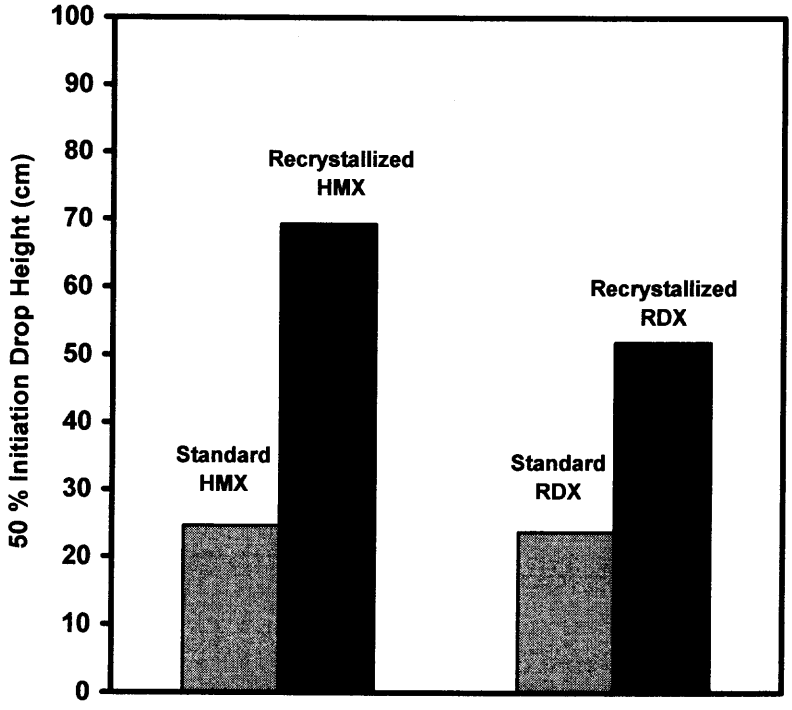

Figure 1.2 Impact sensitivity data obtained from the ERL impact test for standard and recrystallized, ultrafine RDX and HMX. (S. Iyer, V. Stepanov, unpublished).

In this effort, the objective was to develop a method for recrystallization of nitramine energetic materials down to the nano scale (<100 nm). A process was sought such that gram quantities of material could be produced. Consequently, the nano-scale material would be tested for sensitivity to a variety of stimuli and compared to standard powders.

In addition to the reduction of sensitivity, other novel properties may be discovered as a result of reduction of the explosive crystal size. No data describing

production or properties of nanoscale nitramine energetic materials was found. The results of such investigation may pave the way to an entirely novel class of materials with superior properties.

An obvious improvement would be an enhanced burning rate which would result from the tremendous increase of the surface area per unit mass. Assuming spherical particle geometry, a 100 nm particle would exhibit a 1000 fold increase in surface to volume ratio with respect to a 100 μm particle. As illustrated in Figure 1.3 for CL-20, the fraction of surface molecules in a crystal becomes significant as particle size drops below 100 nm.

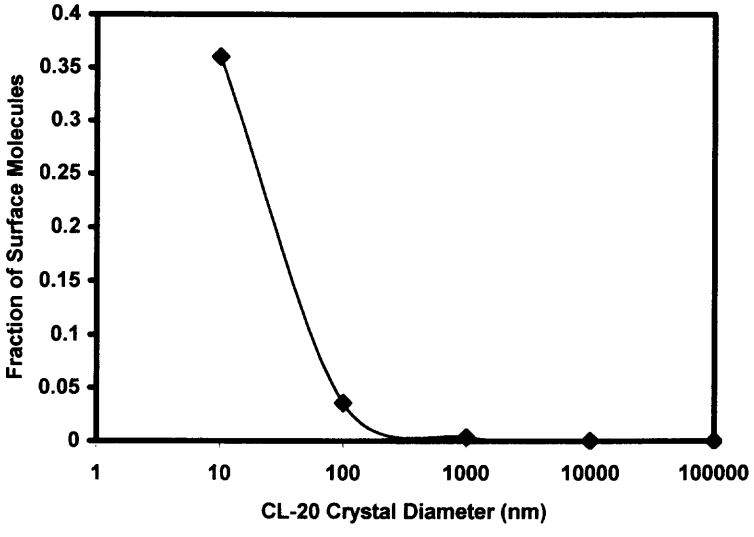

Figure 1.3 Fraction of surface molecules in a crystal of CL-20 *vs.* crystal size.

It is in this size region where significant changes in the inherent physical properties are expected and have been observed in metals, electronics, ceramics, and many other materials. One of the reasons for the change in the properties is that surface molecules are different in nature from internal molecules. On the surface, the range of molecular vibration is less restricted. Thus, larger separation from the equilibrium position is

possible[1]. As the fraction of surface molecules becomes significant, the macroscopic property changes may become more apparent.

A process was sought that would enable the production of nanocrystalline energetic materials with narrow size distribution and high crystal quality. CL-20 was chosen as the material for initial experiments. It was chosen since it is the most sensitive material and has the highest energy density. Desensitization of CL-20 would be of high importance to the energetics community. A variety of potential processes to meet this task were reviewed. These included: spray drying and a variety of supercritical fluid processes including: Rapid Expansion of Supercritical Solutions (RESS), Gas Anti-Solvent Crystallization (GAS), and Precipitation with a Compressed Anti-Solvent (PCA). RESS was chosen as the most suitable process since it most favored particle formation in the sub 100 nm scale.

CHAPTER 2

BACKGROUND

2.1 Supercritical Fluid Processing

The field of supercritical fluid processing is rapidly gaining momentum as new applications and processes are continuously developed and employed. During the past two decades the amount of research in this field has been growing exponentially. Initial experiments with supercritical fluids date as far back as early 19^{th} century. In 1822, Baron Cagniard de la Tour first observed the appearance of the supercritical phase. In 1879, Hannay and Hogarth were first to notice that gases in their supercritical regime are able to dissolve solid materials. Today, numerous processes take advantage of this phenomenon including extraction, crystallization, synthesis, and chromatography.

2.2 Properties of Supercritical Fluids

A substance is considered to be in a supercritical state when its temperature is above its critical temperature (T_c) and the pressure is above its critical pressure (P_c). The critical parameters are unique for each compound. Figure 2.1 illustrates the phase behavior of carbon dioxide. As can be seen in this illustration, the critical point lies at the tip of the liquid / vapor phase boundary. The significance of this is that as the critical point is reached the liquid and the vapor phase merge into a single phase. The two phases merge gradually as the liquid phase expands while the equilibrium gas phase is compressed. At the critical point the density of the two phases becomes identical, and the two phases become one.

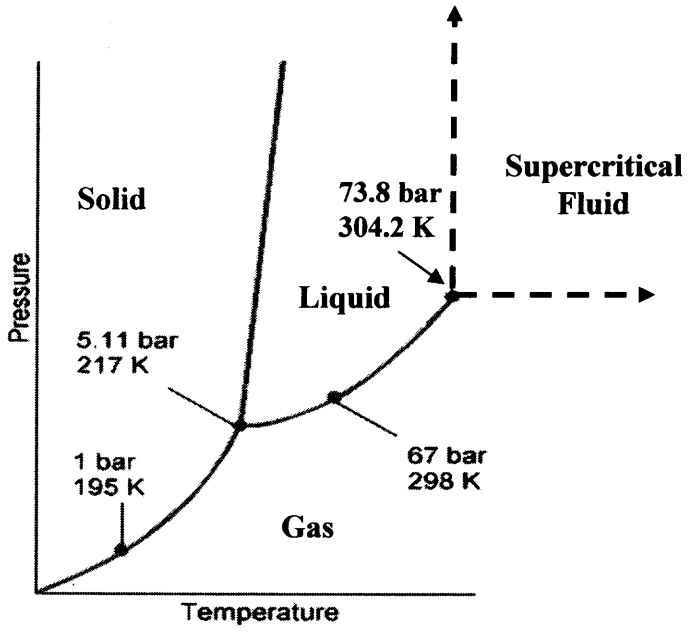

Figure 2.1 Phase diagram of carbon dioxide.

Compounds at a temperature above the T_c are in the gas phase, where condensation into a liquid phase under pressure is no longer possible. Solidification may occur at extreme pressures.

The phase region near the critical point is of most interest, since dramatic changes in properties occur within this region. Specifically, solvation power in this region changes drastically. The primary parameters influencing the solubility are temperature and pressure. As a result, the manipulation of solubility is possible by tuning temperature and pressure, rather than just temperature when dealing with conventional liquid solvents.

Most desired compounds for supercritical fluid processing typically have mild critical parameters, (i.e. $P_c < 100$ bar, $T_c < 100$ °C). Carbon dioxide has been by far the most widely used compound. It has moderate critical parameters, it is an environmentally friendly compound, and it is inexpensive. In food and drug processing it is especially

dominant since products without residual organic solvent may be attained. Table 2.1 lists the most commonly used supercritical compounds and their properties.

Table 2.1 Physical Properties of Commonly Used Supercritical Solvents[2]

Compound	Mol Weight (g / mol)	Critical Temp (K)	Critical Pressure (bar)	Critical Density (g / cm^3)	Critical Compressibility	Accentric Factor
CO_2	44.01	304.19	73.82	0.4682	0.274	0.228
Xe	131.29	289.74	58.4	1.1126	0.286	0
N_2O	44.013	309.57	72.45	0.452	0.274	0.142
H_2O	18.015	647.13	220.55	0.322	0.229	0.345
SF_6	146.056	318.69	37.6	0.7357	0.282	0.215
CHF_3	70.014	298.89	48.36	0.5252	0.259	0.267
$CHClF_2$	86.468	369.3	49.71	0.5209	0.269	0.219
CCl_3F	137.368	471.2	44.08	0.5539	0.279	0.184
$CClF_3$	104.459	301.96	39.46	0.5794	0.283	0.18
NH_3	17.031	405.65	112.78	0.235	0.242	0.252

Solvation power is a major criterion in selecting the proper supercritical solvent. However, cost, safety, and environmental concerns also play a big role. Nitrous oxide has been heavily investigated due to its strong solvent power, however on numerous occasions explosions have been reported and its use has been greatly diminished. Freons also have desirable solvation powers and very mild critical conditions; however, there are environmental issues since Freons are considered ozone depleting and green house gases.

Polarity of the compound is of interest as it affects solubility in a similar manner as it does in conventional solvents. Supercritical fluids with a dipole moment are favored for dissolution of polar compounds while non-polar solvents such as carbon dioxide are favored for dissolution of non-polar compounds.

2.3 Solubility in Supercritical Fluids

Highly compressed gases have the capability of dissolving various materials including solids[3-5]. Solubility becomes appreciable in the near critical region and rapidly increases through the critical point. Beyond the critical point the solubility begins to taper off. This behavior is illustrated in Figure 2.2 depicting the solubility isotherms of RDX.

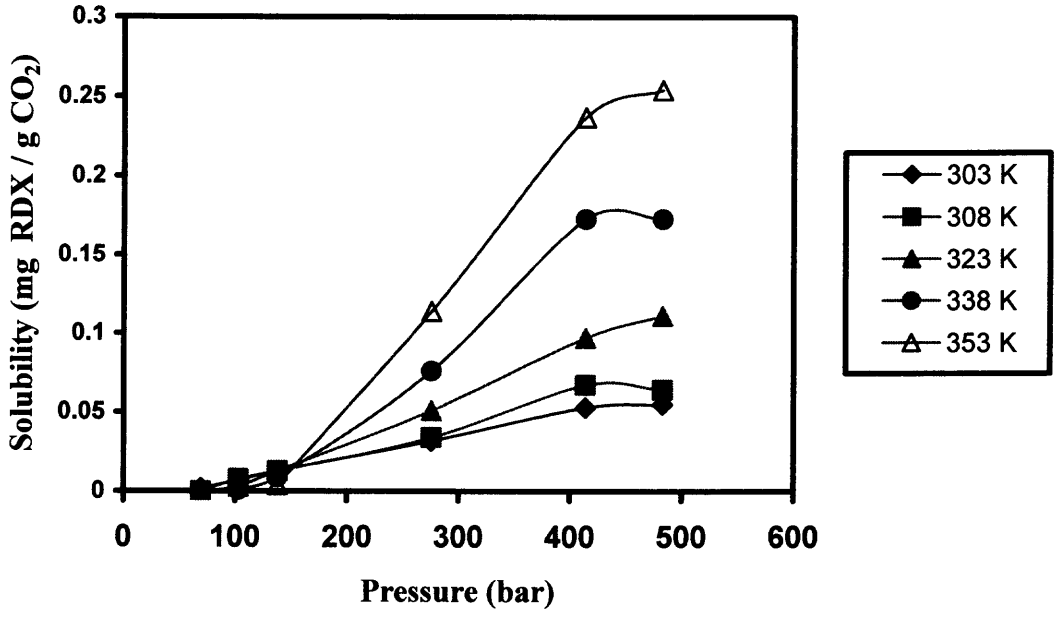

Figure 2.2 Pressure and temperature dependence of RDX solubility in supercritical CO_2[6].

The solvation of a given solute molecule by a compressed gas is a result of clustering of solvent molecules around the solute molecules[7,8]. A typical supercritical solution is highly non-ideal since the mole fraction of the solute in the gas phase far exceeds the amount that would be present due to its vapor pressure alone. The non-ideality is a result of the dense gas with solvation strength approaching liquid values. Thus, even compounds with extremely low volatility such as solids can be dissolved.

Solvation of the solute by clustering of the supercritical solvent around the solute has been experimentally shown. Clustering results in a non-homogeneous fluid density with the density being higher around the solute molecules. Evidence of formation of large solvent clusters around the solute was experimentally gathered by Debenedetti, et al[9]. The clustering was found to be strongest near the critical point. The clustering decreased with deviation from critical point in both directions. Although appreciable solubility in a supercritical fluid can be achieved, the solubilities are usually orders of magnitude lower than for conventional liquid solvents.

The solubility tends to be higher for more volatile compounds. Oils, for example, exhibit much higher solubility than most solids. Knowledge of the solutes vapor pressure usually provides a good indication of the degree of achievable solubility. Most conventional solubility models are formulated around the solutes vapor pressure[10,11]. Temperature, accordingly, is a major factor affecting solubility since the solute vapor pressure increases exponentially with temperature. Similar compounds such as isomers may have orders of magnitude difference in solubility in a supercritical fluid. This difference was found to be closely related to the solutes vapor pressure. It is observed that, in general, for similar solutes one with the greater vapor pressure will exhibit greater solubility.

Another major contributor to solubility is the solvent density. Overall, the solubility trends are as follows: at constant fluid density solubility will increase with temperature, at constant fluid temperature solubility will increase with density.

The significant levels of solubility of non-volatile solutes in dense gases can be interpreted to result from huge enhancement of the solute vapor pressure by the

interaction with the solvent. By considering an ideal gas as a solvent, the expected solubility can be represented by the solid / vapor equilibrium of the solute:

$$y_2 = \frac{p_2^{sat}}{p} \tag{2.1}$$

where y_2 is the mole fraction of the solute in the vapor phase, p_2^{sat} is the equilibrium vapor pressure of the solid and p is the pressure of the system. Such approximation for supercritical mixtures is grossly inaccurate. Here, no solvation effect by the solvent gas is present thus the only amount of solute in the solution is that equivalent to its solid / vapor equilibrium at the given temperature and pressure. If this were the case, only negligible concentrations of solute could be achieved. However, the solvation effect of dense gases is tremendous, and the actual system is far from ideal. At high densities, solvent molecules interact with the solute by clustering around the solute molecules. Such interaction results in significant solvation power. This non-ideal solvation effect can be quantified by introducing the enhancement factor:

$$E = \frac{y_2}{p_2^{sat}/p} \tag{2.2}$$

This expression represents the ratio of the actual concentration of solute in the gas phase versus the concentration in an ideal gas. The value of E is typically very high, reaching values as high as 10^{10} [12,13]. The enhancement is typically correlated according to the widely used equation shown below:

$$E = \frac{\varphi^{o,v}}{\varphi^{v}} exp\left[v^{s}\left(\frac{p - p^{sat}}{RT} \right) \right] \tag{2.3}$$

where

$\varphi^{o,v}$ = solute fugacity coefficient in the reference state

φ^v = solute fugacity coefficient in the vapor phase

v^s = molar volume of the solute

p^{sat} = vapor pressure of solute

p = pressure of the system

The exponential term is known as the Poynting correction factor. This term can be omitted under pressures of around 100 bar. The value $\varphi^{o,v}$ is typically very close to 1, especially for solids. As a result, in most systems, the fugacity coefficient of the solute in the gas phase is of most interest. Values as small as 10^{-6} have been seen in certain systems. This is a clear indication of the high degree of non-ideality in a supercritical solution.

Strong clustering of solvent molecules around the solute is responsible for such great non-ideality. Clustering has been experimentally observed via numerous techniques. It has been seen that around the critical point of the solvent, sharp negative dips in the infinite dilution molar partial volume was present. These values were as large as -16,000 cm^3 / mol [14]. This is directly indicative of condensation of solvent about the solute. Other indications of such solvent clustering include the presence of a shift in the maximum absorption wavelength.

2.4 Cosolvent Modification of Supercritical Solutions

The solubility of polar compounds in a supercritical solvent is typically lower than of non-polar compounds especially when the solvent is non-polar such as CO_2. A common technique for enhancing the solubilities of polar materials in carbon dioxide is the modification of the supercritical fluid with a cosolvent. Conventionally, the cosolvents

are common organic solvents such as acetone, acetonitrile, methanol, etc., that are good solvents for the given solute. Modification with just a few mol % of a cosolvent can result in a solubility enhancement of over two orders of magnitude[15,16].

A modified solution will also have modified critical parameters, thus if working in the near critical region, it should be carefully accounted for in order to avoid the often undesirable two phase regime [17]. The shift of the critical parameters due to cosolvent modification can usually be determined with sufficient accuracy from the arithmetic mean values of the given solvent and modifier:

$$T_c = X_s T_{c(s)} + X_m T_{c(m)}$$
$$P_c = X_s P_{c(s)} + X_m P_{c(m)} \quad (2.4)$$

More accurate results may be obtained from an equation of state such as the Peng Robinson. Table 2.2 indicates such shifts in critical parameters for a set of commonly used cosolvents.

Table 2.2 Effect of Modifiers on the Critical Parameters in Carbon Dioxide

Mole % Modifier	Acetone		Methanol		Ethanol		n-Propanol		i-Propanol	
	T_c (°C)	P_c (bar)	T_c (°C)	P_c (bar)	T_c (°C)	P_c (bar)	T_c (°C)	P_c (bar)	T_c (°C)	P_c (bar)
0	31.3	73.82	31.3	73.82	31.3	73.82	31.3	73.82	31.3	73.82
1	34.7	77.9	32.7	76.5	32.7	76.6	35.5	76.8	34.5	76.2
2	36.8	79.7	34.7	78.2	35.7	78.3	39.1	80.5	37.4	79.3
4	43.7	85.7	37.7	81.7	40.5	84.3	47.2	90	43.5	85.1

Cosolvents are normally chosen that exhibit high solubility as liquids, however, non-solvent liquids are also occasionally chosen. Compounds that are non-solvents as liquids may be effective cosolvents in a supercritical solution. Solvent-solvent interaction in the liquid phase is much stronger than in the gas phase. Water, for instance, exhibits strong hydrogen bonding in the liquid phase, preventing it from dissolving numerous compounds, however, such strong bonding is absent in the gas phase, resulting in novel solvation properties. Non-solvent cosolvents are often desired [18]. Upon expansion of the solution both the solute and the cosolvent will typically precipitate. A non-solvent will not dissolve the final product.

Understanding the miscibility of the modifier with the primary solvent is also of high importance since often excess modifier will result in the formation of a liquid phase[19]. In the case of acetonitrile in carbon dioxide, the amount of acetonitrile should remain below 2 % at pressures below 170 atm. Further addition of acetonitrile results in phase splitting [20].

The solubility of nitramine energetics such as RDX, HMX, and CL-20 is typically very low in supercritical carbon dioxide. This is expected due to the polar nature of these solutes as well their low vapor pressure. It was shown that the solubility of RDX greatly increased in the presence of a modifier[21]. The experiments compared the rate of extraction of RDX with supercritical carbon dioxide, and supercritical carbon dioxide modified by DMSO and acetonitrile at 50 °C and 414 bar. The results show that carbon dioxide modified with 6.1 mol % acetonitrile exhibits a 16 fold improvement in solubility over neat carbon dioxide. Carbon dioxide, modified with 5.6 mol % DMSO, showed an improvement close to 120 times as compared to neat carbon dioxide.

Selection of an optimal cosolvent is a difficult task as both improvement in solvation and separation following extraction are of interest. Thus, a cosolvent with the best solvation may not always be appropriate.

An effective way of choosing the cosolvent with the best solvation power is based on gauging the interaction strength between the cosolvent and the solute. Strong interactions of the cosolvent with the solute are typically a result of hydrogen bonding or charge transfer complex formation. Both mechanisms can fall under Lewis acid-base interaction. J. M. Walsh et al. showed that the interaction strength correlates well with the Lewis acid–Lewis base affinity[22]. The acidity and basicity can be obtained from the solvatochromic parameters α and β respectively. Such data is widely available for most compounds.

2.5 Techniques in Solubility Measurement

A variety of techniques have been developed for the solubility measurement of compounds in supercritical fluids. Most of these techniques fall into three categories: gravimetrical analysis, spectroscopic analysis, and cloud point observation analysis. For highly soluble compounds, gravimetrical techniques and cloud point techniques are sufficient for fairly accurate determination of solubility. However, for compounds with low solubility, spectroscopy is a more reliable approach.

2.5.1 Gravimetric Solubility Analysis

The simplest approach to measuring the solubility of compounds in supercritical fluids is by a gravimetric method[23]. The gravimetric technique normally involves a process where a saturated supercritical solution is prepared at a desired temperature and pressure.

The solution is expanded into a controlled volume and the precipitate is collected and analyzed. The process may be done in a continuous mode or batch mode.

One way of analyzing the collected solute is by weighing. This is typically done with the continuous technique where significantly more precipitate is collected. In a batch arrangement, the precipitate may be collected by dissolving in a liquid solvent. The solution may be analyzed with a spectrophotometer for concentration of solute. A mg or more of collected solute is usually required in order to obtain fairly accurate data. From the weight of the precipitate and the corresponding volume of expanded solution the solubility is determined. The batch mode is by far simpler since equipment such as a high pressure pump is not required. The accuracy of the gravimetric techniques may not be sufficient for slightly soluble compounds (<100 ppm) where only small amounts of solute may be collected. Errors may occur due to various factors, including efficiency of the collection of the precipitate; a fraction is typically lost with the venting gas. Another issue is the carryover of non-dissolved material. This may greatly inflate the actual solubility. These factors become less and less significant for compounds with higher solubility.

2.5.2 Solubility Analysis by Cloud Point Observation

Cloud point observation is the most convenient technique for the solubility determination[24]. This technique requires a high pressure, variable volume view cell. A sapphire window is normally built in to allow visual observation of internal contents. A light source and a camera are mounted on the window and the cell contents are conveniently monitored on a TV screen.

A solution is prepared such that all the solute is fully dissolved. This is visually confirmed by monitoring the solute disappearance inside the cell. Following complete dissolution, the cell is slowly expanded at constant temperature. As expansion takes place, the pressure and density of the solution drop and the solubility begins to decline. Once the saturation point is reached, homogeneous precipitation rapidly occurs resulting in a cloud formation. From the cloud formation conditions over a range of temperatures and pressures a solubility curve is readily prepared. This is one of the fastest ways of solubility measurements since for a single loading numerous saturation points may be determined such as saturation points as a function of temperature and pressure.

This process does not work for slightly soluble compounds since the cloud point below a certain solute concentration is not visible.

Such instrument may also be used to monitor phase behavior of supercritical fluid with a cosolvent. Thus conditions where condensation of the cosolvent occurs may be determined and avoided during solubility measurements.

2.5.3 Spectroscopic Solubility Analysis

Very accurate solubility data may be obtained by spectroscopic analysis. This highly sensitive approach allows solubility determination of slightly soluble materials. A variety of techniques incorporating spectroscopy exist including flow through [6,25] and stagnant modes. Solute concentration is derived from the light absorption by the solute. Normally, the absorption in the ultraviolet (UV) spectrum is studied; however, IR absorption is also a possible alternative.

This kind of analysis requires a high pressure view cell with two windows opposite one another. Absorption of the light is measured by comparing the intensity of

the incident light with that of the emerging light from the view cell. Incident light passes through the cell and absorption of the light by the solute is determined by comparing the intensity of the emerging light with the intensity of the incident light according to:

$$\log \frac{I}{I_o} = -\varepsilon [c] l \tag{2.5}$$

The log of the ratio of the emerging light to the incident light is proportional to the concentration $[c]$ and the length of the optical path (distance between windows) l by the constant ε, which is the molar absorption coefficient[26]. The most appropriate light source for UV radiation is a deuterium lamp because of its stable output intensity. Arc lamps are used when stronger UV intensity is required, however, stability of light intensity is lower than a deuterium lamp. A detector such as a photomultiplier tube (PMT) coupled to a monochromator is one possible approach for light detection. This approach is recommended when single wavelength absorption is of interest. For applications where absorption over a spectrum of wavelengths is required, data collection with a monochromator becomes tedious. A more modern approach is to use an intensified charged coupled device (ICCD) which allows the instantaneous measurement of a wide spectrum of light.

2.6 Techniques in Formation of Ultrafine Particles

A variety of techniques have been demonstrated capable of producing ultrafine particles of organic compounds. A brief review of these techniques is given below.

2.6.1 Spray Drying

The spray drying technique is based on the atomization of a solution of the desired solute and a liquid solvent. The fine aerosol produced by available atomization techniques usually has a droplet size on the scale of 2-10 μm. Next, the mist passes a heating chamber where these droplets evaporate. All the solute precipitates within the droplet as a single particle. The final particle size depends on the droplet volume and the concentration of the solute. Following some basic calculations it was discovered that such process would be very inefficient for production of nano-scale particles. Since the aerosol droplet size cannot be produced smaller than a around a micron, the concentration of the solute would have to be very low. The ratio of solvent to solute would be large rendering the process highly inefficient.

The process allows a highly accurate control of particle size and particles down to a few nanometers can be produced. However, a large volume of solvent will have to be atomized and vaporized to produce a small amount of product. Typically the drying temperature required to achieve rapid droplet evaporation are over 500 °C. Such high temperatures would not be appropriate for use with energetic materials. CL-20 begins to decompose at around 200 °C. Another draw back of spray drying is the common production of undesirable hollow particles[27].

2.6.2 Gas Anti-Solvent Recrystallization

Gas Anti-Solvent Recrystallization (GAS) utilizes a compressed gas such as carbon dioxide as the anti-solvent and a conventional liquid as a solvent[28,29]. This is possible since the solubility of most solids in a dense gas is much lower than solubility in liquids. A liquid solution is initially prepared consisting of the desired solvent / solute system. The solution is then pressurized with the anti-solvent gas. Often, the gas is in its supercritical state, however, gases in subcritical conditions may also be sufficient. Selection of a proper solvent / antisolvent pair is very important as factors like miscibility play a major role in the precipitation process. As the solution is pressurized with the gas, the solution expands. The rate and degree of the expansion are governed by the miscibility of the pair as well as the temperature and pressure. As the solution expands, the solubility rapidly drops and homogeneous precipitation takes place. The crystals are collected by depressurization of the vessel.

Recrystallization with the GAS process results in the formation of fine crystals with highly uniform particle size. Narrow size distribution is attributed to the homogeneous conditions within the solution.

Recrystallization of RDX using the GAS technique was studied by Gallagher et al[29]. Acetone and cyclohexanone were used as solvents. Carbon dioxide was the anti-solvent. It was demonstrated that high quality crystals of RDX with few inclusions, narrow size distribution, and tunable size can be achieved. The particle size is tunable from around 5 microns to hundreds of microns by controlling the rate of pressurization.

Teipel et al. studied the recrystallization of HMX using the GAS process[30]. The smallest mean size was found to be 65 microns for the acetone / carbon dioxide system. Larger crystal sizes were obtained when using γ-butyrolactone as the solvent.

Production of nanoscale crystals with such method would be unlikely as the supersaturation is limited by the slow diffusion process of the gas into the liquid phase.

2.6.3 Precipitation with a Compressed Anti-Solvent Recrystallization

Precipitation with a Compressed Anti-Solvent (PCA) recrystallization is very similar in nature to the GAS process. PCA and GAS are often used interchangeably in the literature. This process involves the addition of a liquid solution to the dense antisolvent gas[31]. Typically, the solution is injected via a nozzle, resulting in microdroplet formation. Selection of a solvent / nonsolvent pair follows similar requirements as for the GAS process. Miscibility, temperature, and solute concentration are of equivalent relevance.

The solution droplets rapidly expand due to miscibility with the dense gas and precipitation takes place. It is believed that the expansion is faster than the bulk liquid expansion in the GAS process due to the higher surface area of the liquid phase. Resulting particle size tends to be smaller in comparison to the GAS process. Submicron particle of organic compounds have been produced using this process. However, particles with sizes below 100 nanometers have not been reported.

2.6.4 Rapid Expansion of Supercritical Solutions

Rapid Expansion of Supercritical Solutions (RESS) is a process that allows the production of particles with smaller size as compared to current GAS or PCA processes. In the RESS process the supercritical fluid is the primary solvent. The solvent power of

the supercritical solvent strongly depends on the pressure or density of the solution. Expansion of a supercritical solution through a nozzle results in a drastic drop in the pressure and temperature. This results in a high supersaturation level of the solute (> 10^6)[32]. Homogeneous nucleation and formation of fine, monodisperse particles follows. The particle size uniformity is a consequence of the highly uniform conditions within the expanding solution[33]. Particle size of organic compounds below 100 nm has been achieved with this technique. For this reason the RESS process was chosen to be the most suitable for this effort. A more detailed description of the process is provided below.

2.7 Mechanism and Thermodynamics of RESS

2.7.1 Expansion of Supercritical Solutions

Rapid Expansion of Supercritical Solutions (RESS) utilizes the strong dependence of solvent power of a supercritical fluid on its density. As a supercritical solution is rapidly expanded, on the order of 10^{-5} sec, a rapid drop in solubility occurs, resulting in a huge supersaturation of the solute (see Figure 2.2). As a result, rapid, homogeneous nucleation and formation of ultra-fine particles with narrow size distribution takes place.

High supersaturation is critical for the production of nano-scale particles or crystals. High supersaturation leads to the homogeneous nucleation of nuclei with very small critical size. In such process a large number of fine nuclei are formed. The nuclei grow and form fully developed crystals within a very short time following the start of expansion.

The RESS process is very sensitive to the operating conditions. The process can be divided into three regions. The pre-expansion region, the nozzle region, and the post-

expansion region. The temperature and pressure in all three region can significantly affect the product characteristics, including size, shape, and morphology. The concentration of the solute in the supercritical solution can also influence the product and is very sensitive to temperature and pressure of the solution. The geometry of the nozzle is another control element of the process. As nozzles vary from short orifice nozzles to long capillary nozzles expansion rates are significantly affected.

The expansion rate has a notable effect on the size of the formed crystals. The expansion rate is directly linked to the achievable supersaturation prior to the start of nucleation. The ability to manipulate the expansion rate is essential to having good control over particle size. Also, the particle morphology may be affected by manipulating the expansion rate. Particles with different shapes such as rod-like, spherical, etc. are often obtained by manipulating the expansion regime[32,34].

The expansion regime may be altered in a number of ways. One of the ways is by changing the pre-expansion and the post-expansion temperature, pressure, and density. Another way is by changing the size and the geometry of the expansion orifice. Both are commonly used and allow control over the expansion characteristics including temperature and pressure profiles.

Two primary kinds of nozzles are micro-orifice nozzles and capillary tube nozzles. Orifice and capillary nozzle sizes are typically in the range of 25 to 150 μm. An important nozzle parameter is the aspect ratio which is the ratio of length to diameter (L / D). Typical L / D values for orifice nozzle are between 3 and 20. Capillary nozzles have much larger L / D values, ranging from around 150 to as much as 6000. A much slower expansion is attributed to long capillary nozzles, approaching 0.1 s, compared to 10^{-6} s

for short orifice nozzles[35]. Depending on the geometry of the nozzle, the expansion velocity can be subsonic, sonic, and supersonic. In order to have subsonic velocity the nozzle must converge along the expansion path, for supersonic velocity the nozzle must diverge, and for sonic velocity a cylindrical geometry is required[35]. Generally, particle size associated with capillary nozzle expansion is substantially larger than that achieved when using micro-orifice nozzles.

The solute concentration in the pre-expansion state will also dramatically influence the level of supersaturation and consequently of particle size and morphology.

The pre-expansion conditions have significant influence on the expansion process. The pre-expansion conditions can be defined as the conditions of the supercritical solution at a location just upstream of the entrance to the orifice, where no significant changers in pressure and temperature have taken place due to expansion. These conditions may be the same or significantly different from the conditions inside the saturation vessel. Typically the effluent solution from the saturation vessel will be heated near or at the nozzle to achieve the desired pre-expansion conditions. Often, the pre-expansion conditions will be different from the conditions inside the saturation vessel. Better control of the pre-expansion conditions in achieved by heating the tubing leading to the nozzle. This is also done to prevent condensation of the solute on the cooler walls of the tubing. When heating the nozzle, it is important to note that if operating in the post retrograde region the solubility of the solute will decrease since the density of the solution will decrease. This may result in premature precipitation of the solute and cause problems such as clogging of tubing and of the orifice.

A rapid pressure drop across the nozzle and beyond is accompanied by a rapid cooling of the solution. The details of expansion cooling are touched upon in the following section. In most cases, the cooling may be assumed to be adiabatic. As the solution cools, condensation of carbon dioxide may take place. Depending on the expansion regime condensation into liquid droplets or directly into solid carbon dioxide can take place. Solvent condensation is not fully understood due to the complex thermodynamics involved, but the implications on the condensation of the solute can be profound.

The degree of solvent condensation during expansion can be reduced by increasing the pre-expansion temperature. This is often necessary since high rate of solvent condensation results in the blockage of the expansion orifice. Most expansion nozzles are designed with incorporated heating elements which help maintain a sufficient nozzle temperature to avoid solid condensation within the nozzle.

A significant amount of expansion and cooling occurs outside the nozzle. In this region, controlling the temperature is much more difficult. In most cases there will be condensation of the expanding fluid and in case of carbon dioxide formation of solid particles. It can be anticipated that some or all of the precipitated solute is temporarily encapsulated in the condensed carbon dioxide. It is unknown whether the solute particles are fully grown at the time of encapsulation. Thus, the mechanism of the solvent condensation and the subsequent evaporation may play an important role on the particle formation process and needs to be further investigated.

The solubility of many organic substances is often very low in supercritical fluids such as CO_2. In order to improve solubility the solution may be modified by adding

organic cosolvents such as acetone, acetonitrile, alcohols, etc. Modifications with even 2 % of cosolvent often show dramatic solubility enhancements.

Although organic cosolvents improve solubility, their use brings up processing difficulties with respect to solvent-product separation and solvent recycling. A major setback to the RESS process with a cosolvent is the condensation of the organic cosolvent followed by re-dissolution of the solid product into the organic phase.

In order to remedy these problems, a number of approaches may be tried. One option would be to use a co-solvent, which is a non-solvent in the liquid phase. Water is known to behave in such manner, thus eliminating the re-dissolution issue. However, for many solutes such cosolvents do not sufficiently improve solubility thus other means must be explored to remedy the condensation of the cosolvent. Heating of the nozzle and of the expansion chamber are critical to the prevention of cosolvent condensation following expansion. Using volatile cosolvents such as acetone reduces the heating required as compared to DMSO or other less volatile cosolvents. At low cosolvent concentrations < 1 mol %, and sufficiently high temperature this may be overcome.

2.7.2 Thermodynamics of Free Expansion of a Compressible Fluid Through a Nozzle

A number of factors need to be addressed in order to describe the cooling of the expanding fluid. Some of the calculations shown below are based on a simplified expansion process. Expansion was taken to be adiabatic, frictionless, and without external pressure or confinement (free expansion). When considering free expansion of real gases, a number of factors must be evaluated to properly understand the thermal behavior of the given system. For a system undergoing adiabatic free expansion, with above assumptions,

the total energy of the system must remain constant. Thus, $E_1(T_1,V_1)$ is equal to $E_2(T_2,V_2)$ with 1 and 2 indicating the initial and final states respectively. To better understand the thermal behavior of the system the total energy (E) can be broken down into two major components:

$$E = E_{thermal} + E_{kinetic} \tag{2.6}$$

Here, $E_{thermal}$ is the internal energy of the gas and accounts for energy of thermal motion as well as the interaction energies of the gas. $E_{kinetic}$ is the kinetic energy associated with unidirectional bulk motion of the gas. Prior to expansion, the gas is confined and all the energy is thermal. During expansion, the thermal energy is converted into kinetic energy thus reducing the value of $E_{thermal}$ resulting in a lowered temperature.

For real gases, a strong dependence of internal energies on volume is often observed. This is based on the partitioning of the energies between the average kinetic and the potential energy terms. For ideal gases with no interactions this factor would be omitted. Such non-ideal behavior is often referred to in terms of the Joule-Thomson coefficient:

$$\mu_{JT} = \left(\frac{\partial T}{\partial P}\right)_H \tag{2.7}$$

The Joule-Thomson coefficient describes the temperature dependence on pressure for isenthalpic expansion or compression. For all compounds, there are (P-T) regions where the JT-coefficient is positive and where it is negative. This has the implications of a gas cooling or heating upon expansion. In order to delineate the regions where μ_{JT} is positive and where it is negative, temperature inversion curves are constructed consisting of loci of solutions of the Joule-Thomson coefficient where it is equivalent to zero. Using

an equation of state, for a range of temperatures the corresponding pressures are evaluated for which the μ_{JT} is zero.

To proceed with such calculation, the expression for μ_{JT} is rearranged into:

$$\left(\frac{\partial T}{\partial P}\right)_H = -\frac{1}{C_P}\left(V - T\left(\frac{\partial V}{\partial T}\right)_P\right) \tag{2.8}$$

For a pressure explicit equation of state the following rearrangement is utilized:

$$\left(\frac{\partial V}{\partial T}\right)_p = -\frac{\left(\frac{\partial P}{\partial T}\right)_V}{\left(\frac{\partial P}{\partial V}\right)_T} \tag{2.9}$$

Substitution into equation 8 results in:

$$\mu_{JT} = -\frac{1}{C_P}\left(\frac{V\left(\frac{\partial P}{\partial V}\right)_T + T\left(\frac{\partial P}{\partial T}\right)_V}{\left(\frac{\partial P}{\partial V}\right)_T}\right) \tag{2.10}$$

All the differential terms are obtained by direct differentiation of the chosen equation of state (EOS).

It is evident that in order for the μ_{JT} to equal 0, the numerator on the right hand side should be 0:

$$V\left(\frac{\partial P}{\partial V}\right)_T + T\left(\frac{\partial P}{\partial T}\right)_V = 0 \tag{2.11}$$

Thus, the temperature inversion curve is calculated by solving equation 11 together with an equation of state. Below derivations utilize the Peng Robinson equation of state:

$$P = \frac{RT}{V-b} - \frac{a(T)}{V^2 + 2bV - b^2} \tag{2.12}$$

where

$$a(T) = 0.45724 \frac{(RT_c)^2}{P_c} \left(1 + k\left(1 - \left(\frac{T}{T_c}\right)^{1/2}\right)\right)^2$$

$$k = 0.37464 + 1.54226\omega - 0.26992\omega^2$$

ω = acentric factor

$$b = 0.07780 \frac{RT_c}{P_c}$$

For a two component system such as the CO_2 / Acetone system, mixing rules were used to derive a and b parameters of mixtures:

$$a = y_1^2 a_1 + y_2^2 a_2 + y_1 y_2 a_{12}$$

$$a_{12} = (a_{11} a_{22})^{0.5} (1 - k_{12})$$

$$b = y_1 b_1 + y_2 b_2$$

k_{12} - mixing parameter

Using the above expressions the temperature inversion curves for CO_2, CO_2 with 2 % acetone and CO_2 with 10 % acetone were calculated.

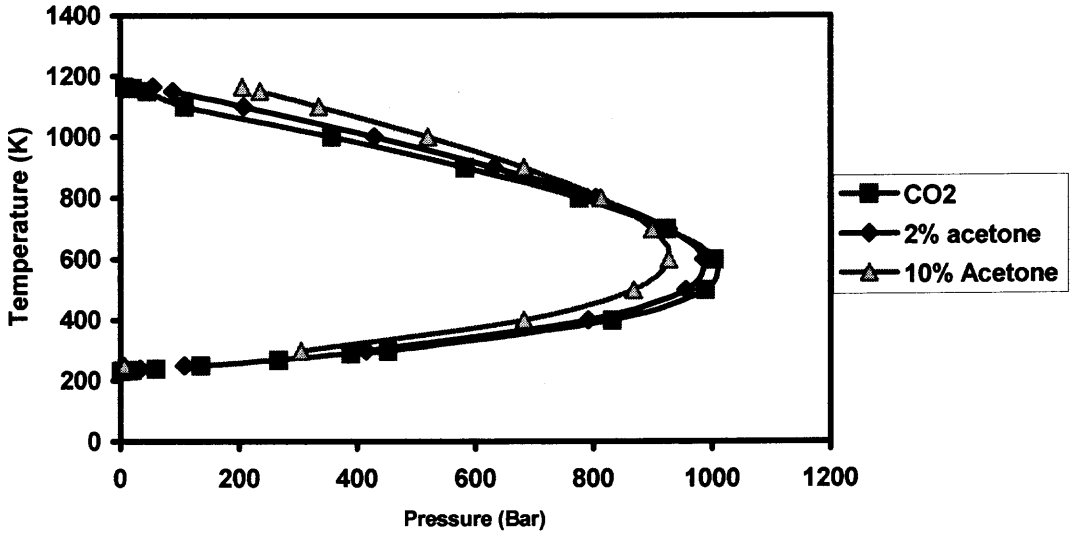

Figure 2.3 Joule-Thomson inversion curves for CO_2 / acetone mixtures.

The effect of acetone on the inversion curves is illustrated in Figure 2.3. It is seen that the effect becomes more pronounced with increasing pressure and temperature. Typical conditions used for supercritical carbon dioxide processing lie well inside the inversion curves.

2.7.3 Jet Expansion from a Nozzle

The jet velocity is strongly governed by the pressure differential between the source tank and the external atmosphere. Important factors to be considered are the conditions of the stagnant fluid inside the tank, the conditions at the nozzle exit and the external conditions. When the pressure differential between the tank and the atmosphere are small the stream velocity is subsonic, however further increasing the pressure difference results in sonic flow at the nozzle exit. The velocity at the nozzle exit may not exceed the sonic velocity thus any further change in the external pressure will not affect the flow velocity.

The flow will only depend on the conditions inside the pressure vessel, since the sonic velocity is dependent on the local pressure and temperature. As the pressure is varied inside the tank so will the sonic velocity.

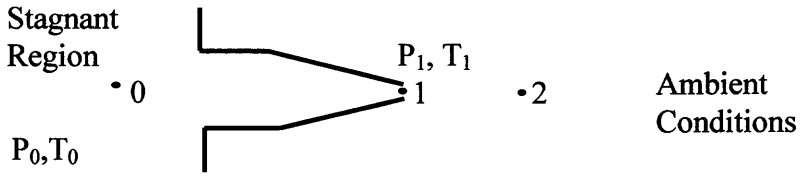

Figure 2.4 Diagram of a converging nozzle.

Figure 2.4 illustrates a converging nozzle. The flow rate can be calculated from the pre-expansion and the post-expansion conditions with the following equations. Since expansion is assumed to be into vacuum the nozzle exit velocity of Mach 1 is used. The Mach number is the ratio of fluid velocity to the sonic velocity. For given pre-expansion conditions of the stagnant gas, conditions at nozzle exit are evaluated using below expressions[36]:

$$\frac{p_0}{p_1} = \left(1 + \frac{k-1}{2} M_1^2\right)^{k/(k-1)} \tag{2.13}$$

$$\frac{T_0}{T_1} = 1 + \frac{k-1}{2} M_1^2 \tag{2.14}$$

$$k = C_p / C_v$$

For a sonic flow M = 1; Equation 2.13 can be rearranged to give the relationship between the nozzle exit pressure and the pre-expansion pressure:

$$\frac{p^*}{p_0} = \left(\frac{2}{k+1}\right)^{k/(k-1)} \tag{2.15}$$

p^* - critical pressure, nozzle exit pressure for sonic flow

Using the pre-expansion pressure the critical pressure may be obtained. Based on the critical pressure flow regime may be obtained:

$$\text{If } p_2 > p^* \text{ flow is subsonic}$$
$$p_2 \leq p^* \text{ flow is sonic}$$

A strong contributing factor to the expansion cooling is the isenthalpic cooling. For such process, the temperature change due to Joule-Thomson effects can be seen from the isenthalp which is calculated from the EOS. Figure 2.5 illustrates such isenthalp for a carbon dioxide / acetone system.

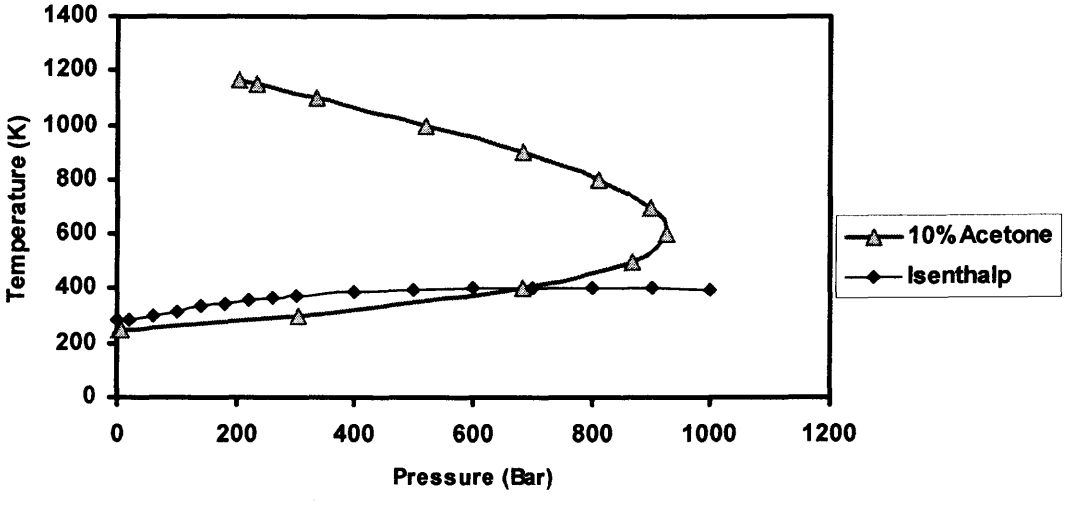

Figure 2.5 Expansion isenthalp for the CO_2 / 10 % acetone system.

The isenthalp illustrates that upon free expansion from 1000 bar and 400 K a rise in the temperature is initially observed. Once the inversion curve is crossed, the temperature begins to drop. A total temperature drop of around 100 K is achieved over the entire expansion path.

2.7.4 Nucleation and Growth of Crystals

Precipitation of a solute from a supersaturated solution is initiated by the formation of nuclei. Consequently, under the appropriate conditions, the nuclei grow into crystals. The nucleation process typically follows one of two mechanisms: homogeneous nucleation or heterogeneous nucleation. Homogeneous nucleation is the predominant nucleation route in the RESS process. Only a small fraction of the fluid is in contact with the nozzle walls during expansion thus the contribution of heterogeneous nucleation is negligible.

In the case of heterogeneous nucleation, the nucleation takes place on a surface of a solid such as the wall of a container or some dispersed particulate matter. Homogeneous nucleation involves the spontaneous formation of embryos which are comprised of the material undergoing nucleation. This happens as a result of spontaneous density or composition fluctuations within the supersaturated solution. In heterogeneous nucleation, the onset of phase transition tends to correspond closely to the equilibrium phase transition as governed by classical thermodynamics. As a result, the metastable zone width is relatively narrow and high supersaturation is very difficult to achieve. The metastable zone in this case refers to extension or overlap of the single phase solution into the two phase region without physically undergoing any phase change as would be required to achieve thermodynamic equilibrium. Such overlap or metastability is almost always the case to a certain extent in phase transitions.

Both heterogeneous and homogeneous nucleation processes require activation. The activation energy is required to overcome the nucleation free energy barrier. This activation energy barrier decreases with increasing supersaturation. Thus, for a highly supersaturated solution a small perturbation is sufficient to bring about precipitation. On the surface of a solid, as is the case of heterogeneous nucleation, nucleation is catalyzed on the solid, reducing the required activation energy and precipitation is facilitated. Thus, in the presence of a solid, nucleation takes place at relatively mild supersaturation.

In the case of homogeneous nucleation, the metastable zone width is much wider. Only at very high supersaturation levels with correspondingly low activation free energy requirements can spontaneous formation of nuclei take place. Here the necessary free energy is derived from local density and composition fluctuations. Nucleation from a highly supersaturated solution is much faster and is more violent as the phase is far removed from its equilibrium conditions. Rapid nucleation results in a large number of fine nuclei. As a result small particles are formed as a product.

The classical nucleation theory, which dates back to the 1920's, is still commonly used to describe nucleation processes. The homogeneous nucleation process is comprehensively covered in *Metastable Liquids* by P. Debenedetti[37], essential aspects were adopted from that work.

Precipitation from a supersaturated solution starts with the spontaneous formation of nuclei. A nucleus often consists of as little as a few dozen or less molecules and is highly unstable. The energetics of the formation of the nucleus is described by the following equation[38]:

$$\Delta W \cong n(\mu_\infty - \mu_1) + \gamma 4\pi r_i^2 \tag{2.16}$$

where

W = reversible work

n = number of molecules in the cluster

μ_∞ = chemical potential of molecules in the condensed state

μ_1 = chemical potential of molecules on the bulk state

γ = surface free energy of the cluster

r_i = radius of the cluster

The second term of this expression accounts for the energy required in the formation of the surface of the nucleus, this term is always positive. The first term describes the energy requirements for the deposition of molecules on the surface of an embryo. For a supersaturated system this term will be negative since the chemical potential of molecules in the bulk state is higher. In a system below the saturation level this term will be correspondingly positive, and the work required for the formation of nucleus will be positive and increasing with the nucleus size. As illustrated in Figure 2.6, the minimum reversible work requirement will reach a maximum for a cluster of a specific size and then decrease. This is a critical cluster size with n* molecules. Any further addition of molecules to a cluster with a critical size or larger will happen spontaneously since the process becomes energetically favorable. However, clusters below the critical size will tend to spontaneously disintegrate. The activation free energy of nucleation is thus the energy required to form a cluster of a critical size.

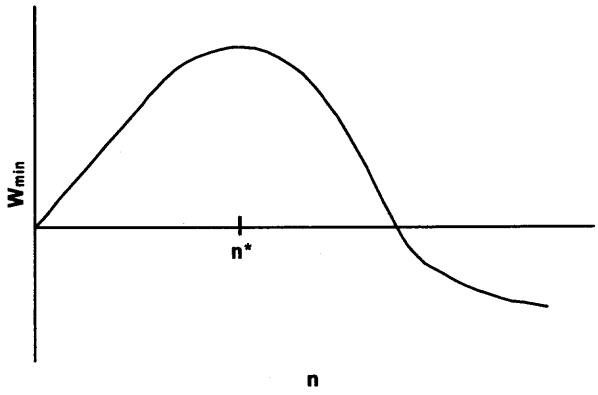

Figure 2.6 Qualitative illustration of the energetics of nucleus formation and growth.

The classical nucleation theory is formulated around the growth kinetics and mechanism of nuclei. The growth process is a competition between the deposition of molecules on the surface of the embryo and the loss of molecules back into the solution. The rate of deposition of single molecules on the surface can be obtained from kinetic theory, however, the rate of the loss of single molecules from the surface is not known. Commonly, the growth rate is determined from the knowledge of equilibrium size distribution of nuclei where the rate of molecule addition is equal to the rate of molecule loss. This is obtained from the energetics of nucleus formation.

The classical treatment of the nucleation process is based on two primary parameters: the nucleation rate *J (nuclei / sec* m^3*)*, and the critical nucleus size *n** (consisting of n* monomers). The following expressions are used to describe the parameters according to the classical nucleation theory formalism.

$$n^* = \frac{32\pi}{3}\left[\frac{(v')^{2/3}\sigma}{(-\Delta\mu)}\right]^3 \tag{2.17}$$

$$J = 2\beta N_{tot}\sqrt{\frac{\sigma(v')^2}{kT}}\,exp\left[-\frac{16\pi}{3}\left(\frac{\sigma(v')^{3/2}}{kT}\right)^3\left(\frac{1}{\ln S}\right)^2\right] \qquad (2.18)$$

v' is the molecular volume in the condensed phase, σ is the surface tension of the embryo, $\Delta\mu$ is the difference of the chemical potentials in the condensed phase and in the solution. β is the flux of molecules onto the surface of the nucleus. N_{tot} is the total number density of the metastable bulk phase. The degree of supersaturation is designated by S.

As seen from Equation 2.17, the size of the critical nucleus has a very strong dependence on the degree of supersaturation, which is implicit in the value of $\Delta\mu$. Thus, as the supersaturation increases the critical nucleus size becomes smaller. The nucleation rate is driven by the degree of supersaturation. Higher supersaturation leads to a faster nucleation rate. This dependence is strong as can be seen in Equation 2.18. Calculations by M. Turk show that the supersaturation in a free jet expansion can reach values around 10^8. The corresponding nucleation rate would be around 10^{26} (cm^{-3} s^{-1})[39].

The nuclei having equal or larger than the critical size continue to grow by solute condensation on the surface of the particles. This process continues until all the solute in the bulk phase is exhausted. Growth may still continue at this point by aggregation of individual nuclei. Both growth stages can influence the morphology of the final particles with respect to characteristics including size, shape, and size distribution.

CHAPTER 3

EXPERIMENTAL

3.1 Solubility Determination by Solute Collection

3.1.1 Experimental Set-up

Several techniques were considered for the solubility determination of nitramines in supercritical CO_2 and cosolvent modified CO_2. Initial solubility determination experiments utilized a gravimetric approach where the precipitate from a known volume of a supercritical solution is collected and the amount determined by spectroscopy. Solubility of CL-20 in carbon dioxide and modified carbon dioxide with acetone and acetonitrile was investigated.

An experimental set-up was devised as follows. A 650 cm^3 high pressure Parr vessel (P_{max}–3500 psig) with an electrical heating jacket, automated temperature controls, magnetic bar stirring, and spring type pressure gauge (10,000 psig) was utilized as a saturation chamber. Temperature of the vessel is measured with a J type thermocouple located inside the vessel. A second high pressure cell with a 21 cm^3 internal volume was utilized for sampling from the saturation vessel. This cell was custom made from a ½ inch Swagelok tee fitting. Two of the end-caps were custom fitted with 1/8 inch tubing by welding. The sampling cell was connected to the saturation chamber through stainless steel 1/8 inch tubing. A high pressure needle valve was placed in line between the two vessels. Heating of the sampling cell was performed with heating tape with a variable voltage transformer. A 300 cm^3 high pressure Parr vessel was connected to the outlet of the sampling cell for the collection of the precipitate. This connection was made through

1/8 inch stainless steel tubing with a high pressure needle valve. The setup is illustrated in Figure 3.1.

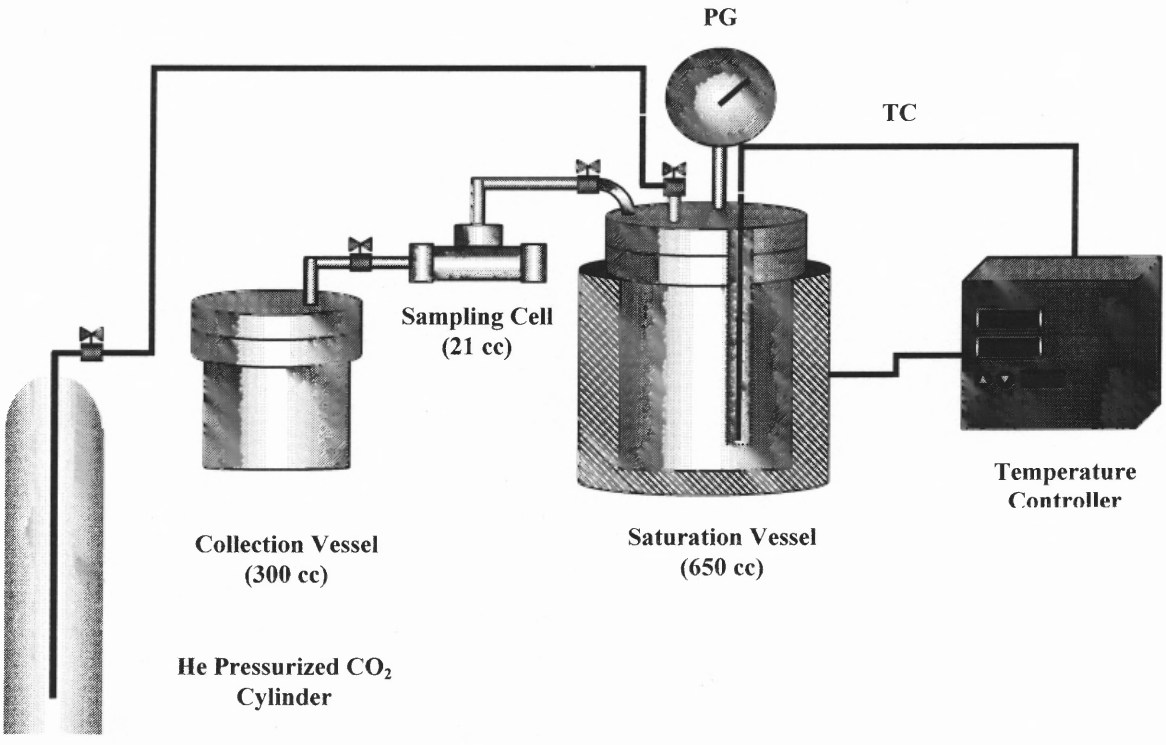

Figure 3.1 High pressure batch set-up for RESS and solubility investigation.

Carbon dioxide was supplied from a helium pressurized (110 atm) supercritical grade liquid CO_2 cylinder equipped with an eductor tube. Helium head pressure is necessary for proper filling of saturation vessel with liquid carbon dioxide. The eductor tube is required so that CO_2 transfer is done directly from the liquid CO_2 phase not the vapor phase which is present at the top of the cylinder. Helium solubility in liquid CO_2 phase was determined to be about 2.5 mol % using mass spectrometry[17].

3.1.2 Experimental Procedure

The solubility measurements were done according to the following procedure. A desired amount of solute powder is loaded into the saturation vessel. The vessel is sealed and flushed to remove air. Flushing was done by filling the vessels with *ca.* 150 psig CO_2, and venting. This is repeated 6 times, leaving ppm levels of air. Next, the saturation vessel is filled with liquid CO_2 at room temperature. Heating of the vessel is initiated and stirring is started. Once the final temperature is reached, the stirring is continued for 3 hours to ensure complete saturation or dissolution. The sampling cell is then heated to the saturation vessel temperature and filled from the saturation vessel with the prepared solution. The contents of the sampling cell are next discharged into the collection vessel.

The precipitate from the expanded solution is collected by washing the sampling cell, the collection vessel, and all the interconnecting tubing and valve with a known volume of acetonitrile. The washing is performed two times. The volume of the recovered acetonitrile is compared with the volume initially measured so that correction can be applied for a more accurate determination of precipitate quantity. The concentration of solute in the acetonitrile wash was determined with a spectrophotometer.

Solubility experiments using a cosolvent are performed somewhat differently. Solution of the solute in the cosolvent is prepared and injected into the flushed saturation vessel. Upon solute recovery, the cosolvent is allowed to fully evaporate prior to washing with acetonitrile. This is especially required when acetone is used as cosolvent. Absorption by acetone in the UV range overlaps with that of CL-20.

Runs without solute were periodically performed in order to determine the background absorption. This background absorption can be mainly attributed to residual

solute from preceding runs and other impurities. Even thorough washing leaves a low level of residue. Subtraction of the background absorption was performed in all runs.

The density of the supercritical CO_2 is calculated form the ideal gas equation of state with compressibility factor correction:

$$\frac{n}{V} = \frac{P}{ZRT} \tag{3.1}$$

where Z is the compressibility factor and R is the gas constant. The values of Z were obtained from empirical tables for CO_2[40]. Densities were thus taken assuming pure CO_2. Contribution of solute is negligible due to low solubility, however, the effect of the cosolvent on the density can be significant.

3.1.3 Spectrophotometric Analysis

CL-20 exhibits strong absorbance in the UV region with λ_{max} at around 225 nm. Thus, spectrophotometry is a potent means for determining the concentration of CL-20 in acetonitrile. Acetonitrile does not exhibit significant absorption in the UV spectrum thus it is an appropriate solvent. A calibration curve for the absorption dependence on concentration at λ = 225 nm was constructed. The extinction coefficient of CL-20 in acetonitrile was determined from the calibration curve. The calibration curve was determined from absorbance data for acetonitrile / CL-20 solutions with different concentrations. The absorbance was plotted vs. concentration (Figure 3.2).

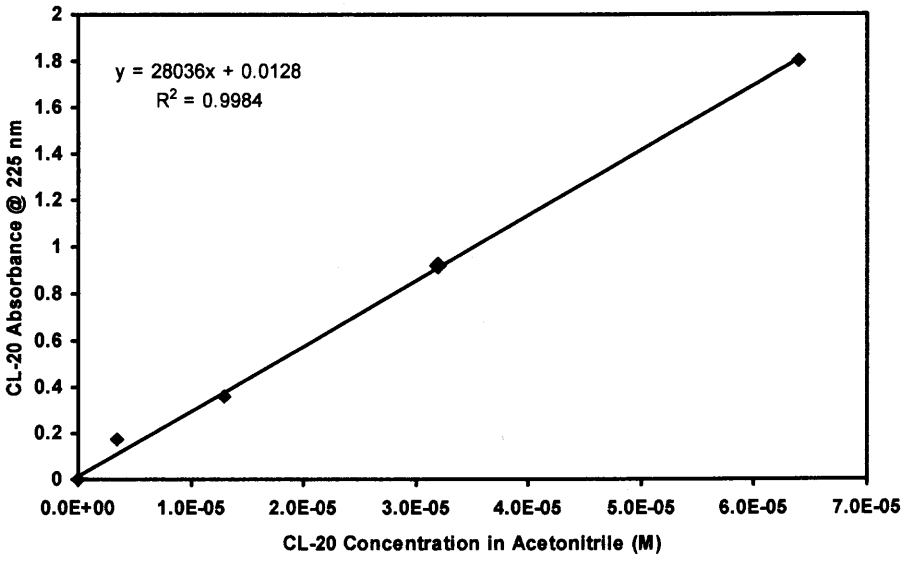

Figure 3.2 Absorption calibration curve for CL-20 in acetonitrile at 225 nm.

The absorbance data is fitted with a linear expression. The extinction coefficient is determined from the Beer-Lambert law:

$$A = \varepsilon [c] l \tag{3.2}$$

Where A is the absorption, ε is the extinction coefficient, c is the concentration of the solute, l is the optical path length. 1 cm cuvettes were used in these measurements, thus l =1. It follows that $\varepsilon = A / [c]$. The extinction coefficient is thus the slope of the fitted line, which is 28,000 M^{-1} cm^{-1} at 225 nm.

3.1.4 Experimental Solubility Data

Solubility of CL-20 was determined in neat CO_2, and CO_2 modified with acetone and acetonitrile at 80 °C and 3,200 psig, the corresponding solvent density is around 0.65 g / cc (Figure 3.3).

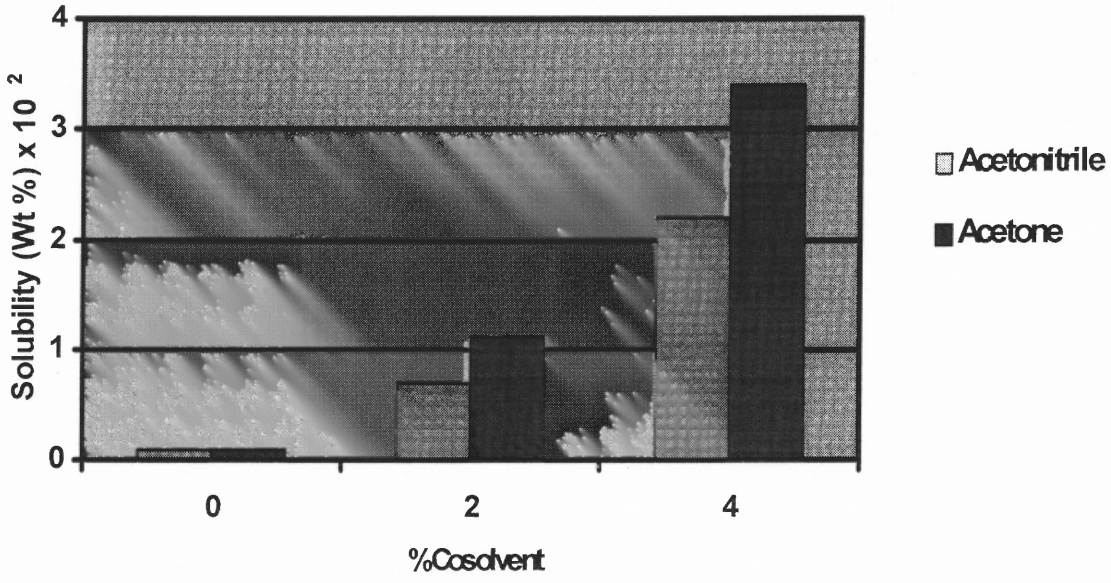

Figure 3.3 Solubility of CL-20 in supercritical CO_2 and modified CO_2 at 80 °C, 3,200 psig.

In order to accurately determine the saturation point at given solvent condition, numerous runs are required. The weight of the loaded compound is plotted vs. collected weight from the expanded solution (Figure 3.4). At the saturation point a plateau is established. From the intersection of the linear fits of the rising mass values vs. plateau values the saturation value is obtained. Such approach was used for the determination of CL-20 solubility in 4 % acetone (mole fraction) modified CO_2 at 80 °C, 3,200 psig. The resulting data points to a saturation concentration of about $3.3x10^{-2}$ Wt %. The accuracy of the plateau value is around ± 10 to 15 %. Such low accuracy can be attributed to numerous factors including the carryover of undisolved material when filling the sampling cell and inconsistencies in collection of the precipitate by washing. Other saturation points, shown in Figure 3.3, were determined by loading excess amounts of solute. The saturation concentration was determined from the recovered amount of solute.

Again, accuracy on the order of ± 10 to 15 % is expected. Although the absolute accuracy of this solubility measurement technique is low, sufficient quantitative and qualitative data on the phase behavior was obtained.

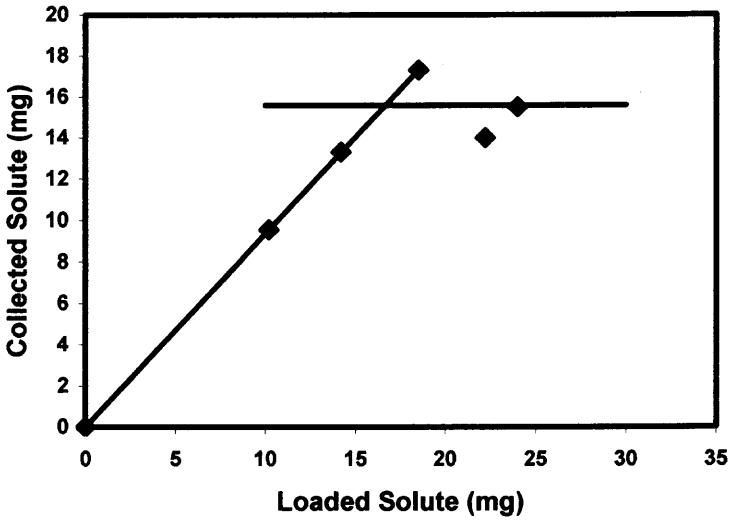

Figure 3.4 Saturation data for CL-20 dissolution in supercritical CO_2 with 4 % Acetone at 80 °C, 3,200 psig.

It can be concluded that the solubility of CL-20 in supercritical CO_2 is below 1 ppm (mole fraction). Addition of cosolvent greatly increases the solubility with resulting solubilities at around 5 ppm. Increasing the fraction of cosolvent had an exponential effect on solubility in the range studies. Doubling the fraction of cosolvent resulted in a three fold increase in solubility with both cosolvents used. Acetone modified solution exhibited *ca.* 30 % solvation higher solubility than for acetonitrile modified solution.

The enhancement factor values were calculated using Equation 2.2 from the experimental solubility data for CL-20. The calculated values are listed in Table 3.1.

Table 3.1 Enhancement Factor Values for Various Supercritical Solutions of CL-20

Solvent	P (psig)	T (K)	E
CO_2 + 4 % Acetone	3200	353	1.97E+08
CO_2 + 4 % Acetonitrile	3200	353	1.17E+08
CO_2 + 2 % Acetone	3200	353	6.15E+07
CO_2 + 2 % Acetonitrile	3200	353	3.94E+07

The vapor pressure was measured by Richard Berhens at the Sandia National Laboratory by a TG-MS technique. Figure 3.5 illustrates the vapor pressure of CL-20 as a function of temperature.

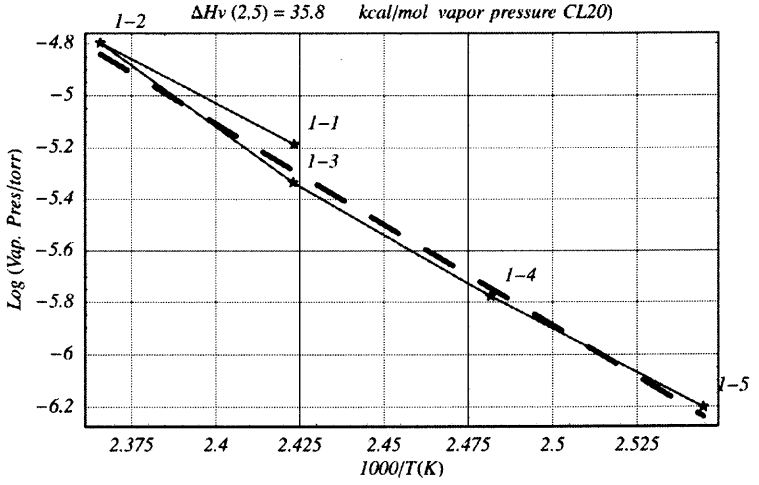

Figure 3.5 Experimental vapor pressure data of CL-20 in the range of 390–420 K.

The following expression was obtained from the fit of the vapor pressure data:

$$\text{Log P (Torr)} = 13.63 - 7807 / \text{T (K)} \qquad (3.3)$$

At 80 °C the vapor pressure as given by the above fit is 3.2×10^{-9} torr.

3.2 Solubility Determination by Cloud Point Observation

3.2.1 Experimental Set-up

Solubility determination of CL-20 and RDX in supercritical CO_2 was also attempted using a Thar Technologies Phase Equilibrium Analyzer. This apparatus allows the determination of the saturation conditions by direct visual observation of the cloud point formation. The cloud point is the rapid onset of nucleation and precipitation in the region of the saturation point. From cloud point data at various temperatures and pressures, the solubility curves can be constructed. A major advantage of this technique is the ability to vary the fluid density during an experiment.

The schematic of the phase analyzer is illustrated in Figure 3.6. The instrument consists of a variable volume view cell, with maximum volume of 25 cm^3. Cell volume is varied with a motor driven piston. A 7/8 inch sapphire window is built into the bottom of the cell. The cell is mounted on a CCD camera which feeds a live image to the TV/VCR. A mechanical stirrer is mounted on the bottom of the piston in the view cell. The view cell is heated through a heating jacket with circulating heating oil from a circulator heating bath. Temperature and pressure reading are directly fed to the PC controller. A software package provides the means to control these process parameters. A syringe pump with internal volume of 300 cm^3 is used to fill the view cell with liquid CO_2 at the desired density. The syringe pump is filled directly from a liquid CO_2 cylinder. This view cell allows operation at a pressure up to 6,000 psig and a temperature up to 130 ^{o}C.

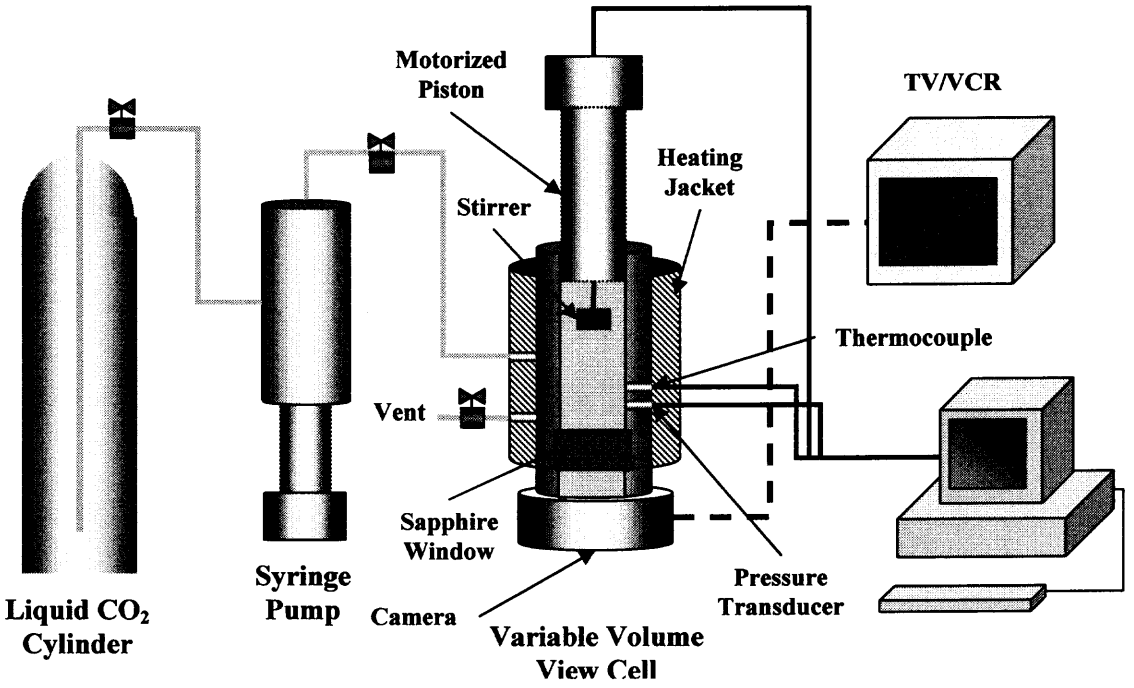

Figure 3.6 Schematic of high pressure phase analyzer.

3.2.2 Experimental Procedure

A desired amount of the solute is weighed and placed inside the view cell. The piston is inserted and sealed. Flushing of the cell to remove air is performed by filling the cell with ca. 150 psi and venting. This is done 6 times to leave ppm levels of air contamination. Before the cell is filled with CO_2, the cell volume is reduced down to 50 to 75 % of the maximum volume. This is necessary so that a wider range of depressurization will be available during the expansion step of the process. The fully expanded syringe pump is filled with CO_2 from the liquid CO_2 cylinder. The valve between the syringe pump and the view cell is open during filling from cylinder. Next the valve to the cylinder is closed and compression of the CO_2 with the syringe pump is initiated. Once the desired pressure is reached, pumping is stopped, and the valve to the view cell is closed. At this point

heating and stirring is initiated. Once the set temperature is reached, manipulation of the view cell volume is possible if higher density or pressure is desired.

The dissolution of the solid which is dispersed on the sapphire window is observed on the TV screen. Once the disappearance of the solid phase is visually observed, expansion of the view cell volume is started by retracting the piston. Expansion rate is controlled with the PC control software. Initial expansion is done at the maximum expansion rate. When the density drops to the saturation point, cloud formation is observed on the TV. In order to more accurately determine the saturation point, the cell is pressurized again to a pressure of a few bar above that where the cloud point was observed. Next the cell is again expanded but at a slower rate. This sequence may be repeated a number of times, each time decreasing the expansion rate, with a more accurate saturation conditions reading. The accuracy of this method is to within a fraction of one bar. One must keep in mind that precipitation does not normally occur exactly at the saturation point, but at the limit of the metastable region where sufficient supersaturation is achieved.

Additional saturation points may be determined without reloading the reactor. This can be done by changing the temperature and repeating the above procedure. Thus numerous solubility points may be determined for a system with a fixed composition.

When cosolvent use is required, normally the cosolvent is added together with the solute. For the solubility measurements, a high pressure Thar P-50 cosolvent pump was connected to the view cell. This allowed in situ augmentation of the cosolvent concentration.

The view cell is typically situated in one of two possible positions. For solids dissolution, normally the cell is fixed in a vertical position. In this case most of the loaded solid is dispersed directly on the window. Following dissolution, the visual observation of the solid disappearance is sufficient for confident confirmation that all of the solid is in solution. Another option is to have the cell in a horizontal position. With solids this is normally undesirable since a difficulty arises in observing the disappearance of the solid phase. However, when working with liquid / gas systems, such as those where a cosolvent is used, or the solute is a liquid, the liquid/ gas interface can be observed. It is important to be able to ensure that only a single phase exists during solubility measurements. In the vertical position separate phases are more difficult to distinguish.

3.2.3 Results

Solubility of CL-20 and RDX was studied at pressures up to 350 bar and temperatures of up to 100 ^{o}C. Acetone was used as cosolvent. The acetone concentration was varied from 2 to 15 %. No observation of a cloud point was made in any of the runs. It was concluded that due to the low solubility of these nitramines the precipitate forming during the expansion process resulted in a low particle concentration, below the level required for visual observation. This technique was determined to be inappropriate for studying systems with solubilities below 10 ppm solute. Proper solubility measurements for CL-20 and RDX would require a spectroscopic technique.

3.3 Particle Formation and Characterization

Particle formation was investigated using the rapid expansion of supercritical solutions (RESS) technique. Two modes of RESS were investigated in these experiments. RESS was done by expansion of supercritical solution through a nozzle and from the sampling cell with characterization of particles collected inside the sampling cell. Both CL-20 and RDX were recrystallized by RESS. Produced particles were characterized using Atomic Force Microscopy and Scanning Electron Microscopy.

3.3.1 Recrystallization by Cell Expansion

3.3.1.1 Procedure. Initial expansion experiments were based on expansion of the supercritical solution from the sampling cell into the expansion vessel through the valve. Set-up and procedure of these experiments is very similar to that used in the solubility determination by solute collection experiments (Figure 3.1). Often, the solubility determination was done simultaneously with particle formation and collection.

Vessel saturation was performed as described in Section 3.2.2. Excess solute would normally be used to ensure full saturation. Following the saturation step, the heated sampling cell was filled with the solution from the saturation vessel. During the sampling cell filling step, the expansion of the fluid from the saturation vessel into the sampling cell results in a significant solute precipitation. 15 to 20 minutes were allowed before expansion of the sampling cell contents in order for the precipitate to redisolve. Expansion of the sampling cell contents is than done by opening the valve leading to the expansion vessel.

Particle collection for analysis was done by placing a glass or mica slide inside the sampling volume. Following the expansion, precipitate collected on the slide, creating

a thin coating of material. In several runs, the sampling was done down stream from the sampling volume, by placing collection slides inside the expansion vessel. No significant amount of precipitate was observed on those slides.

Recrystallization of CL-20 was typically done with cosolvent modified solutions. The presence of a cosolvent such as acetone or acetonitrile caused a number of difficulties. Upon expansion of the solution, significant condensation of the cosolvent occurred. Such condensation is not surprising in light of the large temperature drop of the expanding solution. In some instances sufficient amounts of cosolvent condensation occurred such that product dissolution took place. Most experiments were performed with either 2 or 4 percent of cosolvent. It appeared that when 2 percent of cosolvent was used, at temperatures above 60 °C, condensation was greatly minimized or eliminated. However with 4 percent of cosolvent present, even at 80 °C, the amount of condensate was sufficient to re-dissolve the solid product. As a result, most recrystallization work was limited to systems with 2 % of cosolvent. RDX recrystallization was performed using pure carbon dioxide and modified carbon dioxide.

3.3.1.2 Results. Expansion studies were done for a number of solutions with various pre-expansion temperature and pressure. Effect of the pre-expansion conditions on the particle size and morphology was sought.

CL-20 and RDX particles formed with this mode of expansion ranged in size from 100 nm to few microns. Narrow size distribution was characteristic in the majority

Table 3.2 Experimental Conditions and Results for Cell Expansion Experiments

Exp.	Experimental Conditions						Product Description
	T (°C)	P (psi)	ρ (g/cc)	Solute (mg)	Cosolvent	% Cosolvent	
A-1	55	3400	0.8	CL-20 (21)	Acetone	2	Uniform particles; 420 ± 30 nm
A-2	55	3200	0.8	CL-20 (32)	Acetone	2	Round particles; 40-110 nm
A-3	70	3500	0.7	CL-20 (46)	Acetone	2	Round Particles, 150-900 nm
A-4	65	3550	0.8	CL-20 (44)	Acetone	2	Round paritlces, 200-400 nm
A-5	55	3200	0.8	CL-20 (45)	Acetone	3	Irregular particles; 100-500 nm
A-6	65	3500	0.8	CL-20 (44)	Acetone	4	Large crystals 2-3 μm, irregular shaped particles 250-350 nm
A-7	60	3150	0.8	RDX (56)	None	0	Crystalline particles; 500 ± 180 nm
A-8	70	3600	0.8	RDX (52)	None	0	Elliptical Particles; 170 ± 40 nm

of the samples. Resulting particles appeared to have crystalline structure, as seen by AFM and SEM. Experimental conditions and results are tabulated below.

The collected powder was analyzed using Atomic Force Microscopy (AFM) and Scanning Electron Microscopy (SEM). The size distribution was determined using ImagePro Plus software. The AFM image and size distribution of recrystallized CL-20 by cell expansion are illustrated in Figures 3.7 and 3.8 for experiment A-1. Figure 3.8 shows a three dimensional particle image generated during the AFM analysis.

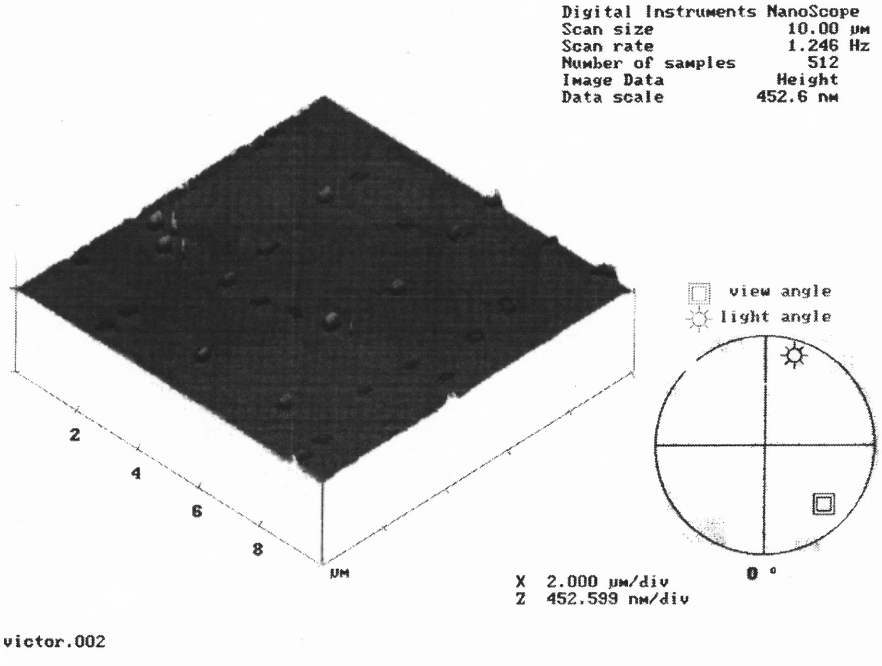

Figure 3.7 3-D AFM image of recrystallized CL-20 by cell expansion from CO_2 + acetone (2%) at 55 °C, 3400 psig. (Experiment A-1).

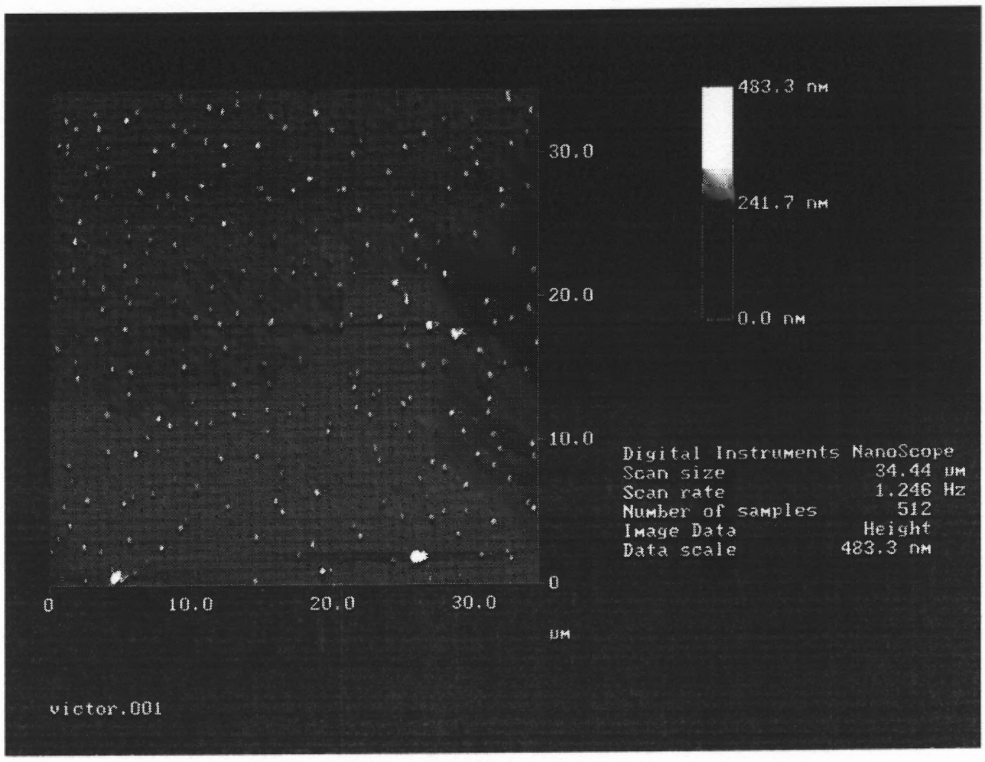

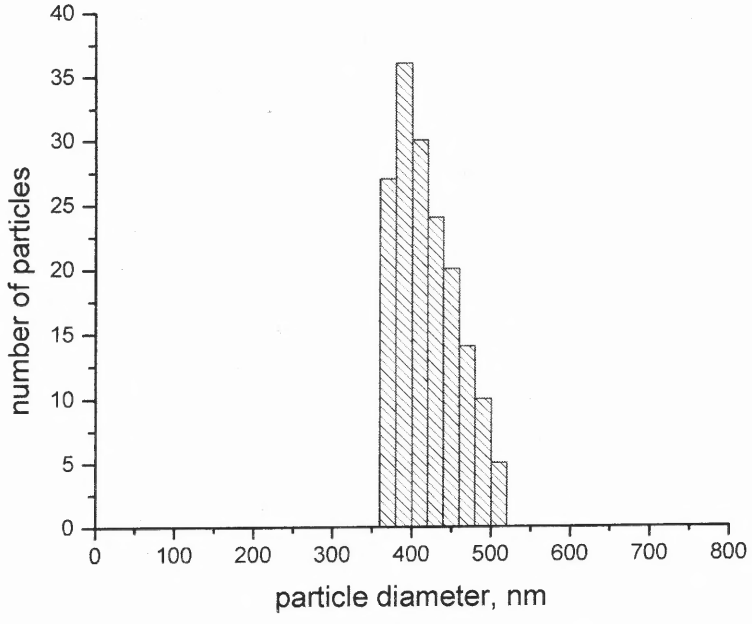

Figure 3.8 AFM image of recrystallized CL-20 by cell expansion from CO_2 + acetone (2%) at 55 °C, 3400 psig. Particle size: 420 ± 30 nm. (Experiment A-1).

A product with very narrow size distribution is observed as can be seen in the histogram. The size distribution follows a lognormal profile, which has been seen in almost all of the experiments. A longer tail is present for particle with larger sizes. Such phenomenon is well known in aerosol formation literature[41]. It is unclear whether this is the true particle size distribution. As the particles are collected on the sampling slide, size discrimination is a possibility. The collection of larger particles will be more efficient than of smaller particles. This is a direct result of the sedimentation time, which is longer for smaller particles. Mean CL-20 particle size was determined to be 420 ± 30 nm. It is difficult to confidently determine from the AFM images whether the particles are crystalline or not. This is a result of poor resolution of the AFM technique. Upon close examination, crystal edges appear to exist. Thus a preliminary conclusion is that the particles are crystalline.

After initial analysis with the AFM, it was decided that SEM analysis would improve the characterization quality of the fine powders. Most of the subsequent analyses were done using a Field Emission Scanning Electron Microscope. Figure 3.9 depicts recrystallized RDX from a carbon dioxide solution at 60 °C and 3150 psig.

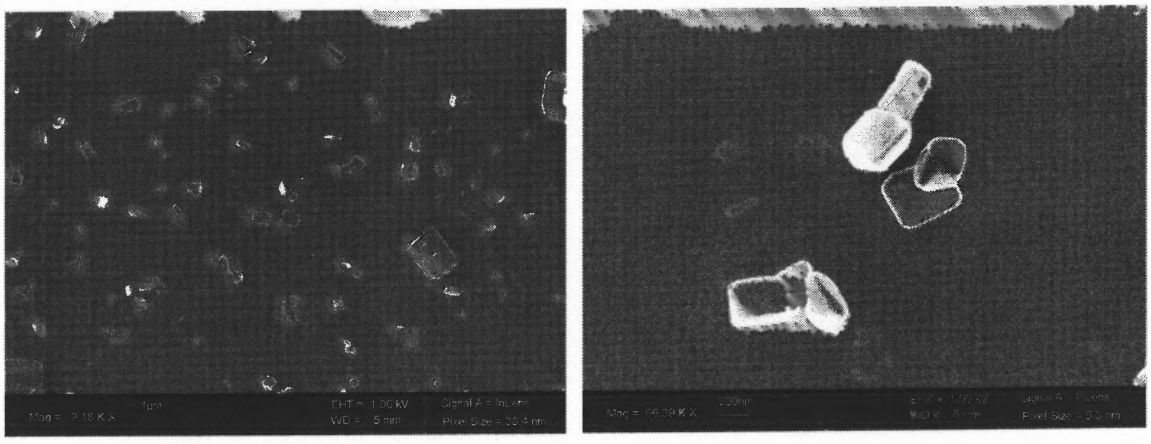

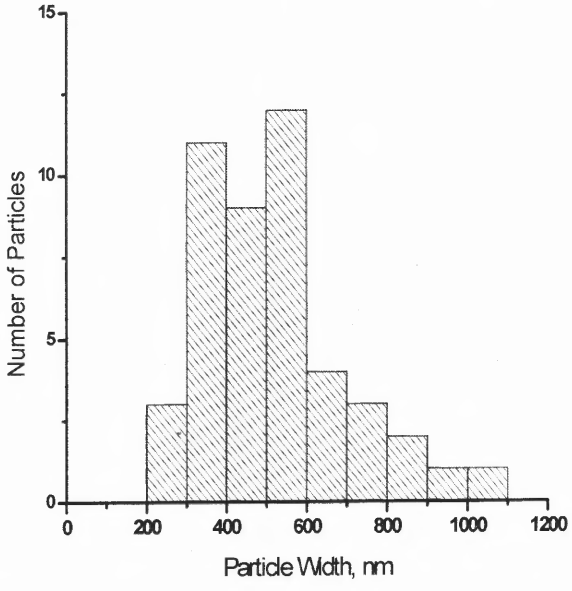

Figure 3.9 SEM images and size distribution profile of recrystallized RDX from CO_2 at 60 ^{o}C and 3150 psig. Particle size: 500 ± 180 nm. (Experiment A-7).

It is evident from Figure 3.9 that SEM provides a significantly higher image resolution. The flat crystal surfaces are indicative of crystalline morphology. Again a lognormal size distribution was observed in the analysis. The mean size was determined to be 500 nm with a standard deviation of 180 nm.

Another Experiment, A-8, was performed in order to determine the effect of temperature on the particle size. The conditions were similar to experiment A-7,

however, the saturation vessel temperature was 10 °C higher. The pressure was correspondingly higher, 3,600 psig, however, the density was kept constant for the two experiments. Such temperature difference may not strongly influence the expansion characteristics such as the expansion rate and the temperature drop. The solute concentration should be significantly higher, as much as 50-60 % increase should be observed from the solubility data in Figure 2.2. Both solutions were stirred for 3 hours prior to expansion. It is believed that full saturation was achieved in this time.

The product of Experiment A-8 was analyzed by SEM. The image is depicted in Figure 3.10. The particles were found to have elliptical shape. Particle size was 170 ± 40 nm. It is evident that the 10 °C increase in temperature had a dramatic effect on the particle size. A smaller size would be expected from a solution with the higher concentration since a higher supersaturation can be achieved upon expansion and thus, a higher nucleation rate. According to the classical nucleation theory, the particle size is inversely proportional to the nucleation rate. A narrower size distribution is also apparent. Resolution of the image is of lower quality than Figure 3.9. This is a result of smaller particle size. It is difficult to tell from this SEM image whether the product is crystalline or amorphous.

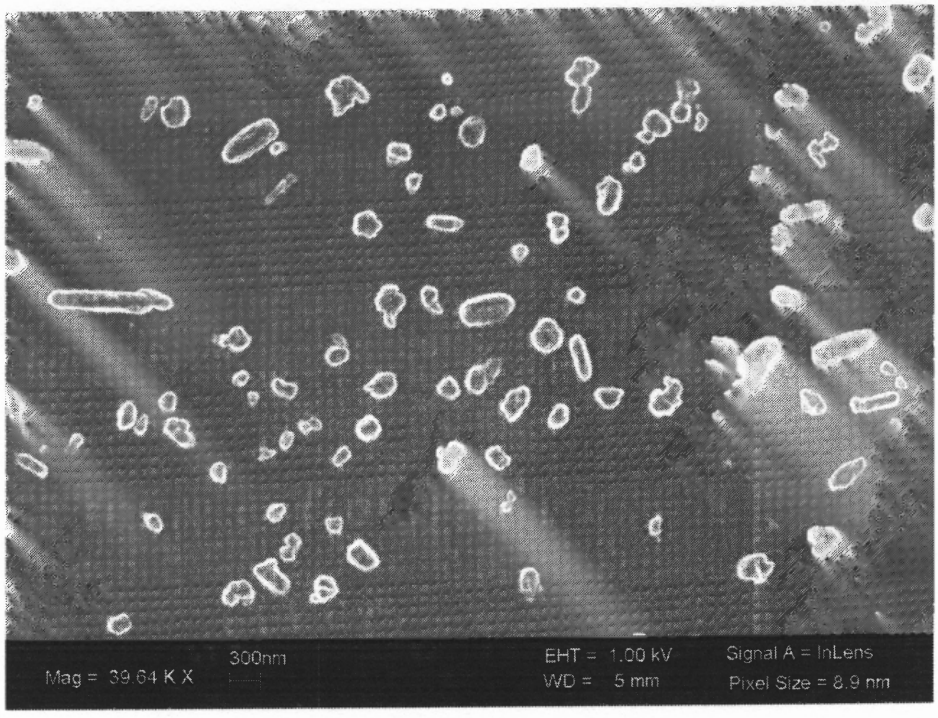

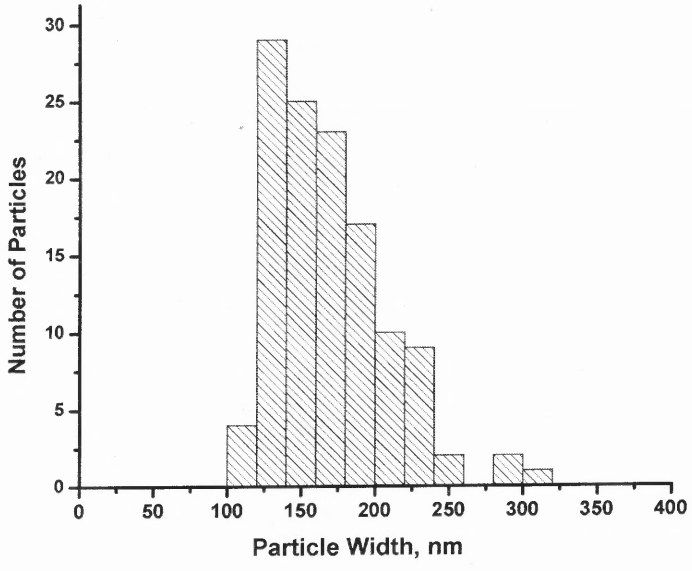

Figure 3.10 SEM images and size distribution profile of recrystallized RDX from CO_2 at 70 °C and 3600 psig. Particle size: 170 ± 40 nm. (Experiment A-7).

Much larger crystals were obtained from experiment A-6. It is clear from the SEM image in Figure 3.11 that the particles are crystalline. Smaller particles with sizes around 250 – 350 nm were also observed on the sample. The overall size distribution had a bimodal character.

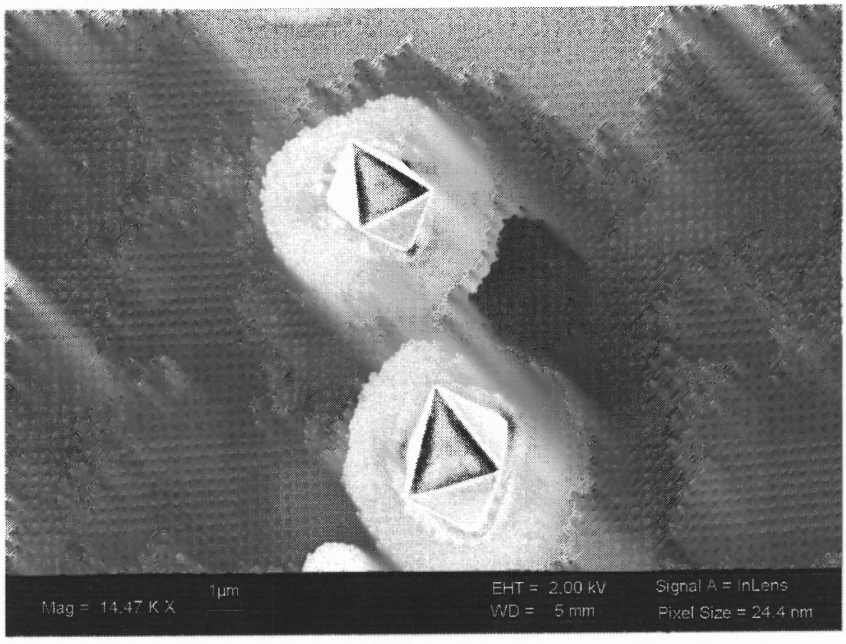

Figure 3.11 Large crystals of CL-20 from cell expansion at 65 °C, and 3500 psig. (Experiment A-6).

3.3.2 Expansion through a Nozzle

Numerous recrystallization experiments were also performed with expansion through a nozzle. The experimental conditions are significantly different from the cell expansion experiments. The cell expansion experiments study the particles which are formed within the sampling volume upon expansion through the valve. Only the particles that precipitate inside the sampling cell are collected, not the particles which are formed downstream. The pressure drop inside the cell is significantly slower than the pressure

drop in the expanding jet. Thus, the nozzle expansion experiments focus on particles which are formed in a much faster expansion environment.

Initial experiments were done by batch expansion. Subsequently a continuous apparatus was assembled and utilized for preparation of larger product amounts.

3.3.2.1 Experimental Set-up. In the batch experiments the set-up described in Section 3.1.1 was used with the following modifications. The sampling cell was removed from the set-up. A nozzle was fitted to the lid of the expansion vessel. 1/8 inch stainless steel tubing connected the nozzle to the output valve on the saturation vessel. The transfer line was wrapped with heating tape and heated to the saturation vessel temperature. Glass slides were placed on the bottom of the saturation vessel for sample collection.

The nozzle used in the experiments was made from a Swagelok ¼ inch brass end plug. A 125 μm orifice was mechanically drilled through the plug.

For continuous operation a system as illustrated in Figure 3.12 was assembled.

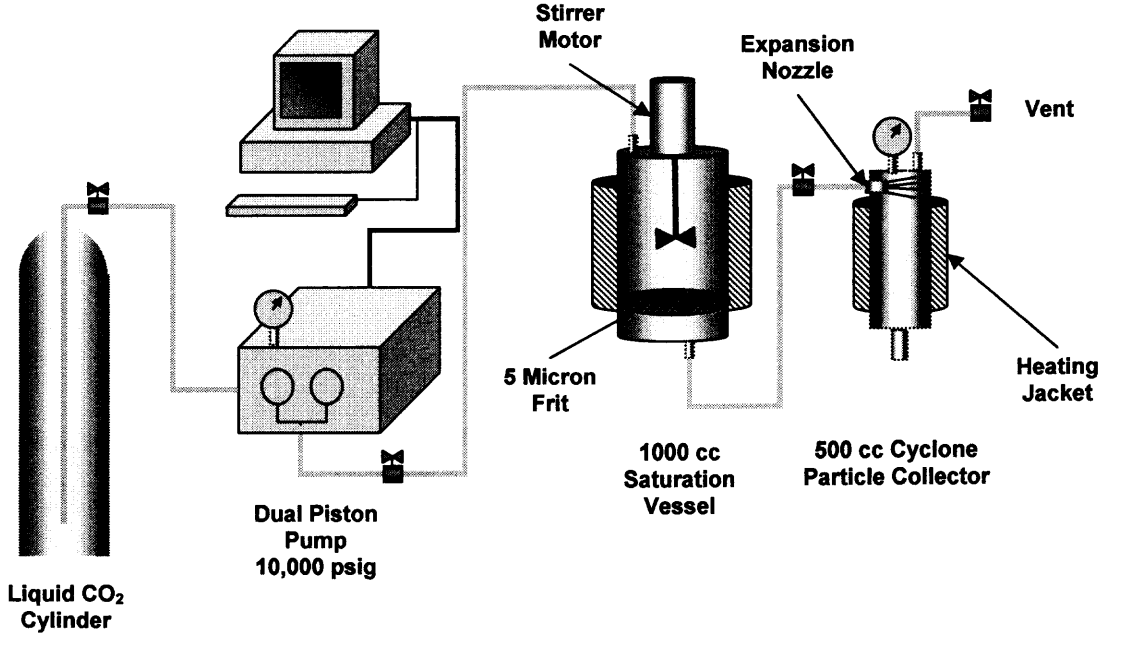

Figure 3.12 Continuous RESS configuration.

Saturation takes place inside the 1000 cm^3 heated high pressure vessel. Rapid mixing is achieved with a powerful stirring system. At the bottom of the vessel a five micron frit is incorporated to avoid transfer of undisolved material. Glass wool is used downstream from the frit for trapping of fine particulates. CO_2 is pumped to the saturation vessel via a Thar P-200 dual piston pump, capable of delivering up to 200 g / min of CO_2 at up to 10,000 psig. In order to achieve efficient pumping, the CO_2 from the cylinder is chilled to about a 5°C inside a heat exchanger cooled by a chiller. Various pumping regimes are available including flow regime and pressure regime, where the pumping is automatically adjusted according to the set parameters.

A second heat exchanger is located downstream from the pump in order to preheat the CO_2 to the desired operating temperature. The heated CO_2 enters the 1000 cm^3 saturation vessel from the top lid. The solution leaves the vessel from the bottom lid of the vessel. All connecting tubing is 1/8 stainless steel heavy walled tubing. The output of the saturation vessel is directly fed to the expansion nozzle, nestled inside the particle collection cyclone. The orifice used in this setup is laser drilled sapphire disk compressed in heated stainless steel housing. The orifice diameter is 100 microns.

The cyclone particle collector consists of a 500 cm^3 vessel rated at 100 bar. The vessel is heated via electrical heating jacket. A back pressure regulator is connected downstream of the cyclone. This allows maintaining up to 15 bar pressure inside the cyclone during operation. The design of the cyclone is such that the particles produced from the expanding jet a driven to the bottom of the vessel by the centrifugal force, while the gas exits at the top of the vessel.

A second pump, Thar P-50, is available for the continuous pumping of a cosolvent at a maximum flow rate of 50 grams per minute. All the pumping and heating is regulated via PC controller with software provided by Thar Technologies.

3.3.2.2 Procedure. In the batch expansion mode, saturation of the tank was performed as described in Section 3.2.2. Following saturation, expansion of the solution into the expansion vessel was done by opening the outlet valve on the saturation vessel. The transfer line and the expansion vessel were heated with heating tape to the same temperature as the saturation vessel. This is necessary to avoid any condensation on the transfer line as well as to avoid cosolvent condensation inside the expansion vessel, where condensate could redisolve the solid product. Expansion was done to atmospheric pressure by keeping a vent line open on the expansion vessel. Sample collection wad done by placing glass slides (1 cm^2) on the bottom of the expansion vessel.

In the continuous mode all experiments were performed without a cosolvent. This was done in order to eliminate the possibility of cosolvent precipitation and dissolution of the product. This measure limited the experimentation to RDX only. RDX solubility in carbon dioxide is sufficient to generate and collect sufficient amount of powder. CL-20 solubility in carbon dioxide alone is insufficient.

A desired amount of powder is loaded inside the saturation vessel. In some of the experiments the powder was manually ground in order to achieve a larger surface area and thus faster saturation. Large excess of powder was also typically loaded for faster saturation. In addition to the 5 micron frit, glass wool is packed in the exit port from the vessel to trap the particles.

All the vessels are heated prior to pumping carbon dioxide. Once the set temperatures are reached, pumping of the CO_2 to the saturation vessel is started. Initially the vessel exhaust is closed. Around five minutes is typically required to fill the saturation vessel with desired amount of CO_2 at the desired pressure (typically 250-300 bar). Once the desired pressure is set inside the vessel, stirring is started and 15-20 minutes is allowed to saturate the vessel before starting the expansion process.

After beginning the expansion process, the backpressure regulator on the cyclone particle collector is adjusted to have around 10-15 bar pressure inside the separator. This pressure is desired to improve the heating of the nozzle. Without heating, the nozzle temperature rapidly drops and clogging of the nozzle is observed from the build up of solid carbon dioxide (dry ice). The CO_2 pump is adjusted in order to maintain a given pressure inside the saturation vessel.

3.3.2.3 Results. A series of experiments were done on CL-20 recrystallization from CO_2 solution with 2% acetone modifier by batch expansion. Another set of experiments were made on recrystallization of RDX from neat CO_2. The experimental conditions and results are tabulated in table 5.

Experiments B-1 through B-4 were performed by batch expansion through a nozzle. The brass nozzle (125 μm diameter) was used. Experiments C-1 through C-3 were performed in a continuous expansion mode. The sapphire disk nozzle (100 μm diameter) was used in experiment C-1 and C-3, the brass nozzle was used in experiment C-2. Recrystallization of RDX was done without any modifier since the solubility of RDX is sufficiently high in neat CO_2. Analysis of particles was done using SEM imaging.

Table 3.3 Experimental Conditions and Results for Nozzle Expansion Experiments

Exp.	Experimental Conditions						Product Description
	T (°C)	P (psi)	ρ (g/cc)	Solute (mg)	Cosolvent	% Cosolvent	
B-1	70	3100	0.7	CL-20 (17)	Acetone	2	Round particles; 100-600 nm
B-2	70	3650	0.8	CL-20 (46)	Acetone	2	Large crystals 2-3 μm, irregular shaped particles 300-800 nm
B-3	70	3500	0.8	CL-20 (46)	Acetone	2	Elliptical particles; L x W 200-300 x 90-125 nm
B-4	70	3550	0.8	RDX (53)	none	0	Large, flat, trapezoidal crystals; 3-4 μm
C-1	75	4000	0.8	RDX (500)	none	0	Uniform, elliptical particles; 120 nm mean width
C-2	75	3900	0.8	RDX (5000)	none	0	Elliptical particles; 460 ±190 nm
C-3	70	4000	0.85	RDX (5000)	none	0	Elliptical particles; 140 ± 40 nm

In the batch recrystallization of CL-20 (experiments B-1 through B-3), large variation of particle size and shape was observed for the experiments with similar conditions. Experiment B-3 resulted in the finest particles. The SEM image of particles produced in Experiment B-3 is shown in Figure 3.13. Two kinds of particles were produced in this experiment; elliptical particles with a width ranging from 90 to 125 nm and length ranging from 200 to 300 nm.

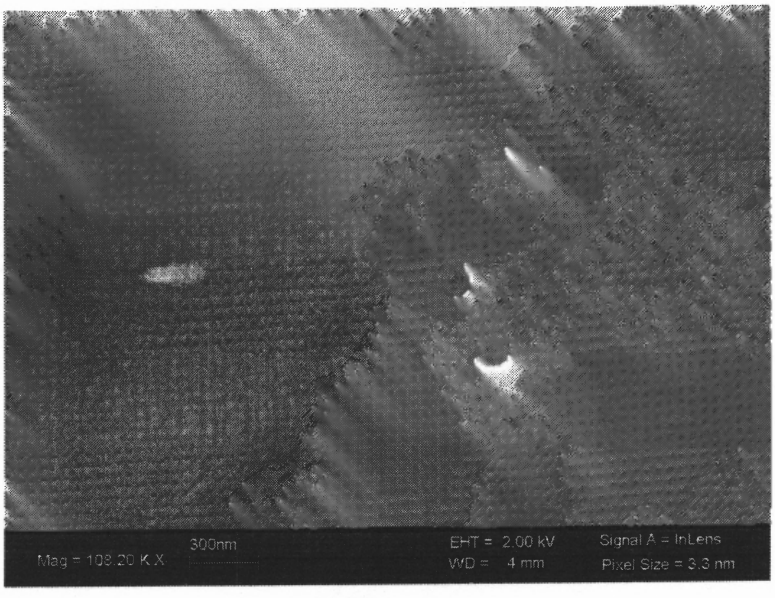

Figure 3.13 SEM image of recrystallized CL-20 from CO_2 at 70 °C and 3500 psig. (Experiment B-3).

A number of continuous recrystallization experiments were performed with RDX. No modifiers were used in this set of experiments. Recrystallization of RDX in the continuous mode expansion using the sapphire disk nozzle (experiment C-1) resulted in small particles with a narrow size distribution. The mean particle size was measured to be 124 nm with a standard deviation of 26 nm (based on measurement of 100 particles). The SEM image and the size distribution curve are shown in Figure 3.14. Both round and

elliptical particles can be seen from the SEM. It is unclear whether the particles are crystalline.

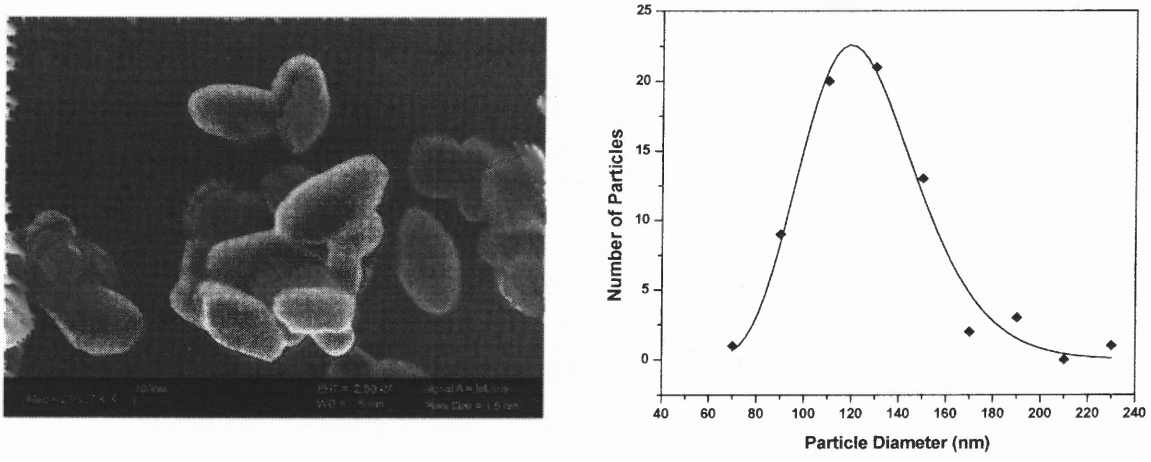

Figure 3.14 SEM image and fitted size distribution curve of recrystallized RDX from CO_2 at 75 °C and 4000 psig. Particle size: 124 ± 26 nm. (Experiment C-1).

Fitting of the particle size data revealed that the distribution follows a lognormal profile. This is consistent with the size distribution seen in the batch experiments and the cell expansion experiments.

Experiment C-2 was performed similarly to Experiment C-1, however the RDX powder was initially ground to increase the surface area, and a larger amount of RDX was placed in the saturation vessel. This was done to increase the saturation level during the expansions process. Larger particles resulted in Experiment C-2 with a wider size distribution (Figure 3.15). Significantly larger amount of product was produced in Experiment C-2 than Experiment C-1. Over 100 mg was collected from the cyclone separator.

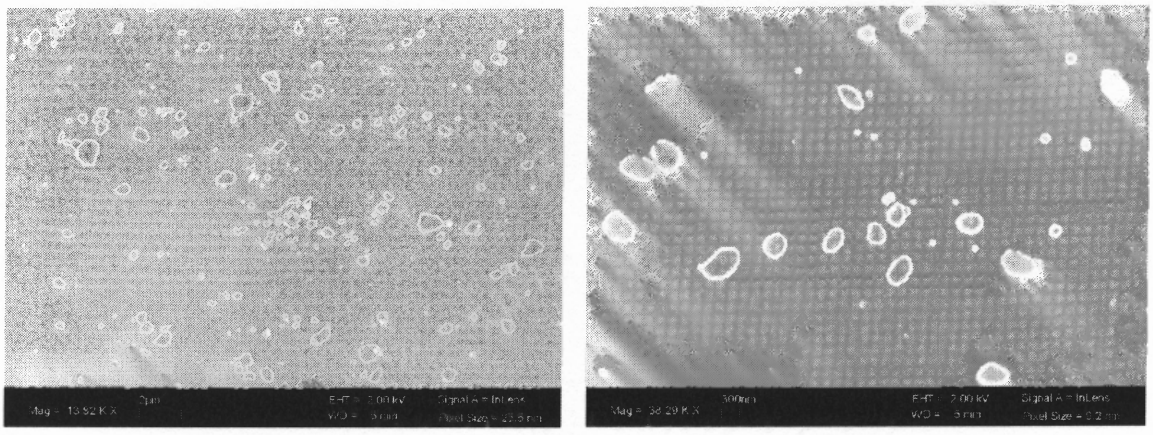

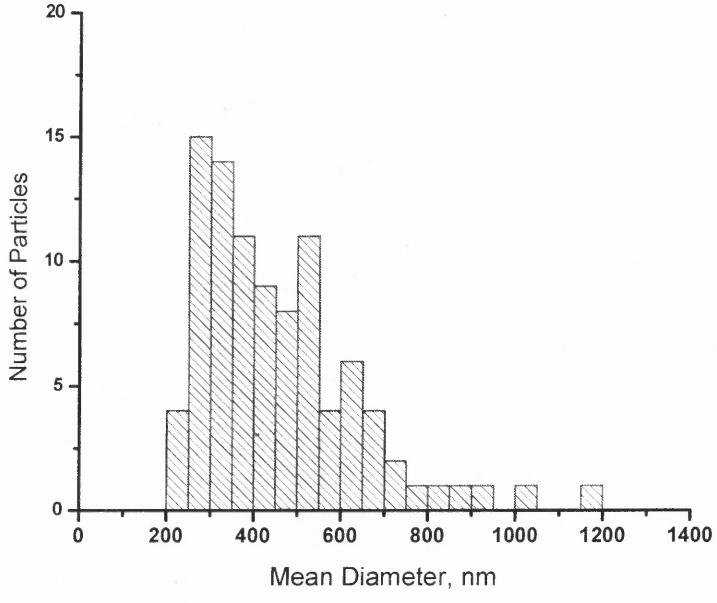

Figure 3.15 SEM image and size distribution profile of recrystallized RDX from CO_2 at 80 °C and 4000 psig. Particle size: 460 ± 190 nm. (Experiment C-2).

The wider size distribution can be partly attributed to the fluctuation in the jet flow rate at the nozzle. Periodic blockage and clearing of the nozzle was observed throughout the experiment. It is evident that clogging was due to accumulation of dry ice in the nozzle.

Experiment C-3 was performed with the sapphire nozzle. The nozzle was heated during the process at 60 °C. This was a sufficient temperature to eliminate nozzle

clogging with dry ice. Without clogging, a more uniform expansion was observed. The SEM image and the particle size distribution is illustrated in Figure 3.16. Fine particles having elliptical shape are seen in the SEM image. The size distribution is significantly more narrow than for the product of Experiment C-2. This is attributed to the better flow uniformity.

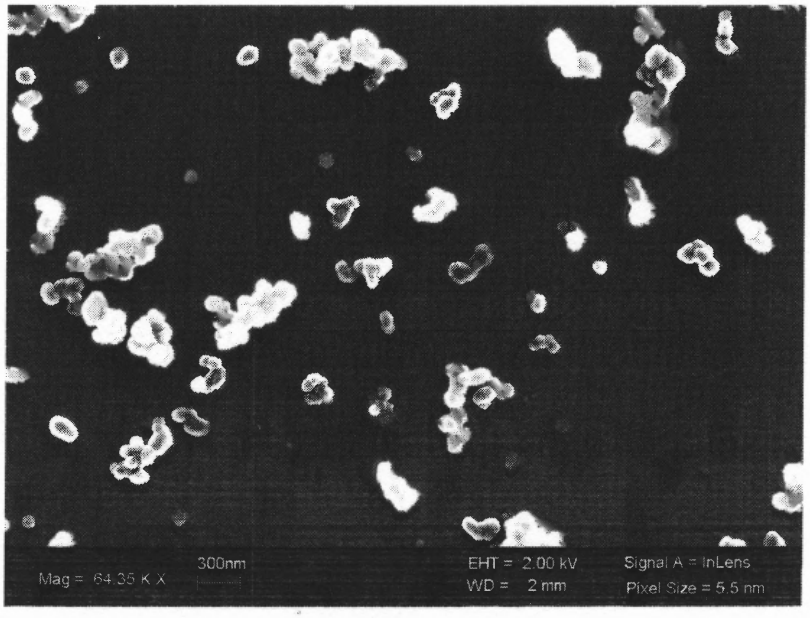

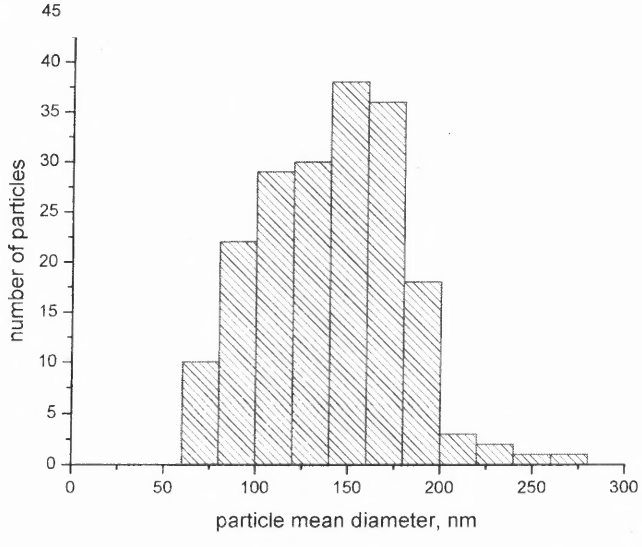

Figure 3.16 SEM image and size distribution profile of recrystallized RDX from CO_2 at 70 ^{o}C and 4000 psig. Particle size: 140 ± 40 nm. (Experiment C-3).

CHAPTER 4

SUMMARY

In this effort, a key task was to determine the feasibility of producing nanocrystalline nitramine energetic materials, including RDX and CL-20. A number of techniques were reviewed. Recrystallization by Rapid Expansion of Supercritical Solutions (RESS) was determined to be the most suitable. Carbon dioxide was chosen as the primary solvent. Acetone and acetonitrile were used as cosolvents.

Initially, a batch set-up was designed and built to perform solubility and recrystallization studies with the RESS process. Solubility of CL-20 was experimentally determined in carbon dioxide and modified carbon dioxide with acetone and acetonitrile at 2 and 4 mol %. The morphology and size of the precipitated crystals were studied. The dependence of crystal characteristics on process conditions including temperature, pressure, and cosolvent type and amount were investigated. Characterization of crystals was done using Atomic Force Microscopy and Scanning Electron Microscopy.

It was observed that in general the particle size decreased with increase in solute concentration. This is consistent with the classical nucleation theory as well as reported trends in the literature.

A continuous RESS set-up was designed and built. This provided the capability for the production of sub-gram quantities of ultra-fine nitramine powders. Optimization of the continuous process was performed. This included the improvement of particle collection, supercritical solvent saturation, and nozzle expansion conditions. Operation with a heated nozzle resulted in a more uniform particle size than the unheated nozzle. The flow out of the heated nozzle was found to be more uniform as clogging by dry ice was eliminated. As a result, formation of powders with a narrow size distribution was achieved.

This effort demonstrated that the production of particles of nitramine energetic materials including RDX and CL-20 with a mean size near 100 nm and narrow size distribution is possible with the RESS process.

Future research direction would be focused on increasing the production capacity of nano-powders by the RESS process. One significant issue that limits the production capacity is the low solubility of nitramines in carbon dioxide. Attempts were made to overcome this limitation by introducing cosolvents. It was demonstrated that with a few mol % of acetone or acetonitrile cosolvents, the solubility can be increased by over two orders of magnitude. However, the addition of a cosolvent brought about another difficulty. It was observed that upon expansion of the cosolvent modified solution the cosolvent would precipitate together with the solute and redisolve the solute. Better understanding of the phase behavior along the expansion path of the ternary systems would be required in order to tune the process conditions such that condensation of the cosolvent can be avoided.

Another issue is the collection of the nanoscale powders. It was realized that precipitation of the fine powders from the effluent gas is extremely slow due to the light weight of the particles. As a result, majority of the powder was believed to have been lost with the venting gas rather than collecting inside the cyclone separator. The cyclone separator was found to be ineffective as none of precipitate was collected on the bottom of this vessel. The precipitate was mainly found at the top of the vessel near the exit port.

The process was found to be very sensitive on the experimental conditions as reproducibility was difficult. Better control of the process conditions such as the temperatures, pressures, and solute concentration would be required.

REFERENCES

1. C. P. Poole Jr. and F. J. Owens, *Introduction to Nanotechnology*, Wiley-Interscience, 2003.

2. C. L. Yaws, *Chemical Properties Handbook*, McGraw-Hill, 1998.

3. K. D. Bartle, G. F. Shilstone, S. A. Jafar, and A. A. Clifford, "Solubilities of Solids and Liquids of Low Volatility in Supercritical Carbon Dioxide," *J. Phys. Chem. Ref. Data*, vol. 20, pp. 713-756, 1991.

4. F. P. Lucien and N. R. Foster, "Solubilities of Solid Mixtures in Supercritical Carbon Dioxide: a Review," *Journal of Supercritical Fluids*, vol. 17, pp. 111-134, 2000.

5. P. G. Debenedetti and S. K. Kumar, "The Molecular Basis of Temperature Effects in Supercritical Extraction," *AIChE Journal*, vol. 34, pp. 645-657, 1988.

6. J. B. Morris, "Solubility of RDX in Dense Carbon Dioxide at Temperatures between 303 K and 353 K," *J. Chem. Eng. Data*, vol. 43, pp. 269-273, 1998.

7. R. S. Mohamed and G. D. Holder, "High Pressure Phase Behavior in Systems Containing CO_2 and Heavier Compounds with Similar Vapor Pressures," *Fluid Phase Equilibrium*, vol. 32, pp. 295-317, 1987.

8. F. Trabelsi, K. Abaroudi, and F. Recasens, "Predicting the Approximate Solubilities of Solids in Dense Carbon Dioxide," *Journal of Supercritical Fluids*, vol. 14, pp. 151-161, 1999.

9. P. G. Debenedetti, N. A. Collins, and S. Sundaresan, "Disproportionation of Toluene over SZM-5 under Near Critical Conditions," *AIChE Journal*, vol. 34, pp. 1211-1214, 1988.

10. G. N. Escobedo-Alvarado, S. I. Sandler, and A. M. Scurto, "Modeling of Solid-Supercritical fluid phase equilibria with a cubic equation of state-G^{ex} model," *Journal of Supercritical Fluids*, vol. 21, pp. 123-134, 2001.

11. P. Coutsikos, K. Magoulas, and G. M. Kontogeorgis, "Prediction of solid-gas equilibria with the Peng-Robinson equation of state," *J. of Supercritical Fluids*, vol. 25, pp. 197-212, 2003.

12. P. G. Jessop and W. Leitner, *Chemical Synthesis Using Supercritical Fluids*, Wiley-VCH, 1999.

13. K. P. Johnston and C. A. Eckert, "An Analytical Carnahan-Starling-vad der Waals Model for Solubility of Hydrocarbon Solids in Supercritical Fluids," *AIChE Journal*, vol. 27, pp. 773-779, 1981.

14. J. F. Brenecke and C. A. Eckert, " Fluorescnence Spectroscopy Studies of Intermolecular Interactions in Supercritical Fluids," *AICHE Annual Meeting,* Washington, DC, pp. 14-26, 1988.

15. M. P. Ekart, K. L. Bennet, S. M. Ekart, G. S. Gurdial, C. L. Liotta, and C. A. Eckert, "Cosolvent Interactions in Supercritical Fluid Solutions," *AIChE Journal*, vol. 39, pp. 235-248, 1993.

16. S. T. Ting, D. L. Tomakso, S. J. Macnaughton, and N. R. Foster, "Chemical-Physical Interpretation of Cosolvent Effects in Supercritical Fluids.," *Ind. Eng. Chem. Res.*, vol. 32, pp. 1482-1487, 1993.

17. E. M. Glebov, L. G. Krishtopa, V. Stepanov, and K. L. N., "Kinetics of a Diels-Alder Reaction of Maleic Anhydride and Isoprene in Supercritical CO_2," *J. Phys. Chem. A*, vol. 105, pp. 9427-9435, 2001.

18. K. Mishima, K. Matsuyama, D. Tanabe, S. Yamauchi, T. J. Young, and K. P. Johnston, "Microencapsulation of Proteins by Rapid Expansion of Supercritical Solution with a Nonsolvent," *AIChE Journal*, vol. 46, pp. 857-865, 2000.

19. C. Day, C. J. Chang, and C. Chen, "Phase Equilibrium of Ethanol + CO_2 and Acetone + CO_2 at Elevated Pressures," *J. Chem. Eng. Data*, vol. 41, pp. 839-843, 1996.

20. L. T. Taylor, *Supercritical Fluid Extraction*, John Wiley & Sons, Inc, 1996.

21. J. B. Morris, " Supercritical Fluid Extraction of Triple-Base and LOVA Gun Propellants," *JANNAF,* San Diego, CA, 1999.

22. J. M. Walsh, G. D. Ikonomou, and M. D. Donohue, "Supercritical Phase Behavior: the Entrainer Effect," *Fluid Phase Equilibrium*, vol. 33, pp. 295-314, 1987.

23. M. A. McHugh and V. J. Krukonis, *Supercritical Fluid Extraction: Principles and Practice*, Butterworth-Heinemann, 1994.

24. J. M. Lee, B. Lee, and S. Hwang, "Phase Behavior of Poly(l-lactide) in Supercritical Mixtures of Carbon Dioxide and Chlorodifluoromethane," *J. Chem. Eng. Data*, vol. 45, pp. 1162-1166, 2000.

25. M. J. Carrott and C. M. Wai, "UV-Visible Spectroscopic Measurement of Solubilities in Supercritical CO_2 Using High Pressure Fiber-Optic Cells," *Anal. Chem.*, vol. 70, pp. 2421-2425, 1998.

26. P. Atkins, *Physical Chemistry*, W. H. Freeman and Company, New York, 1994.

27. K. Okuyama and I. W. Lenggoro, "Preparation of Nanoparticles via spray route," *Chemical Engineering Science*, vol. 58, pp. 537-547, 2003.

28. J. C. de la Fuente Badilla, C. J. Peters, and J. de Swaan Arons, "Volume Expansion in Relation to the Gas-Antisolvent Process," *Journal of Supercritical Fluids*, vol. 17, pp. 13-23, 2000.

29. P. M. Gallagher, M. P. Coffey, and V. J. Krukonis, "Gas Anti-Solvent Recrystallization of RDX: Formation of Ultra-fine Particles of Difficult-to-Comminute Explosive," *Journal of Supercritical Fluids*, vol. 5, pp. 130-142, 1992.

30. U. Teipel, U. Forter-Barth, and H. Krause, "Crystallization of HMX-Particles by Using the Gas Anti-Solvent Process," *Propellants, Explosives, Pyrotechnics*, vol. 24, pp. 195-198, 1999.

31. J. Jung and M. Perrut, "Particle Design Using Supercritical Fluids: Literature and Patent Survey," *Journal of Supercritical Fluids*, vol. 20, pp. 179-219, 2001.

32. P. G. Debenedetti, "Homogeneous Nucleation in Supercritical Fluids," *AIChE Journal*, vol. 36, pp. 1289-1298, 1990.

33. P. G. Debenedetti, R. S. Mohamed, and R. K. Prud'homme, "Effects of Process Conditions on Crystals Obtained from Supercritical Mixtures," *AIChE Journal*, vol. 35, pp. 325-328, 1989.

34. K. Ohgaki, H. Kobayashi, and T. Katayama, "Whisker Formation from Jet of Supercritical Fluid Solution," *Journal of Supercritical Fluids*, vol. 3, pp. 103-107, 1990.

35. Y.-P. Sun, *Supercritical Fluid Technology in Materials Science and Engineering*, Marcel Dekker Inc., 2002.

36. R. H. Perry, D. W. Green, and J. O. Maloney, *Perry's Chemical Engineers' Handbook*, 7th ed. McGraw-Hill Professional, 1997.

37. P. G. Debenedetti, *Metastable Liquids*, Princeton University Press, 1996.

38. R. P. Andres, " Homogeneous Nucleation in a Vapor,", in Zettlemoyer A.C., (ed): *Nucleation,* Marcel Dekker Inc., 1969.

39. M. Turk, "Influence of Thermodynamic Behavior and Solute Properties on Homogeneous Nucleation in Supercritical Solutions," *Journal of Supercritical Fluids*, vol. 18, pp. 169-184, 2000.

40. S. Angus, B. Armstrong, and K. M. de Reuck, *International Thermodynamic Tables of the Fluid State: Carbon Dioxide*, in Pergamon Press, Oxford, 1976.

41. H. R. Pruppacher and J. K. Klett, *Microphysics of Clouds and Precipitation*, D. Reidel, 1978.